Journal of Medicinal Chemistry

Article

pubs.acs.org/jmc

Gold-Containing Indoles as Anticancer Agents That Potentiate the Cytotoxic Effects of Ionizing Radiation

Sandra Craig,[†] Lei Gao,[‡] Irene Lee,[‡] Thomas Gray,*[,‡] and Anthony J. Berdis*[,†]

[†]Departments of Pharmacology and [‡]Chemistry, Case Western Reserve University, 10900 Euclid Avenue, Cleveland, Ohio 44106, United States

Supporting Information

ABSTRACT: This report describes the design and application of several distinct gold-containing indoles as anticancer agents. When used individually, all gold-bearing compounds display cytostatic effects against leukemia and adherent cancer cell lines. However, two gold-bearing indoles show unique behavior by increasing the cytotoxic effects of clinically relevant levels of ionizing radiation. Quantifying the amount of DNA damage demonstrates that each gold−indole enhances apoptosis by inhibiting DNA repair. Both Au(I)−indoles were tested for inhibitory effects against various cellular targets including thioredoxin reductase, a known target of several gold compounds, and various ATP-dependent kinases. While neither compound significantly inhibits the activity of thioreoxin reductase, both showed inhibitory effects against several kinases associated with cancer initiation and progression. The inhibition of these kinases provides a possible mechanism for the ability of these Au(I)−indoles to potentiate the cytotoxic effects of ionizing radiation. Clinical applications of combining Au(I)−indoles with ionizing radiation are discussed as a new strategy to achieve chemosensitization of cancer cells.

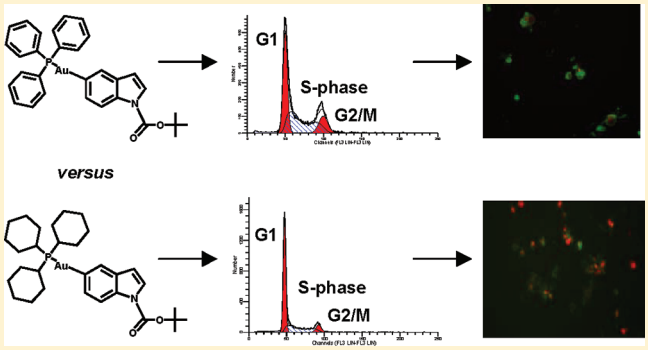

INTRODUCTION

Metals such as magnesium, iron, and cobalt play essential cellular roles in biological systems by performing catalytic roles in biochemical reactions.[1−3] However, other metals including copper, gold, and platinum possess properties such as redox reactivity, Lewis acidity, variable coordination modes, and reactivity toward biological macromolecules that can unleash lethal effects on cells.[4−6] The toxicity of these metals can, under certain conditions, be controlled and subsequently used to efficiently kill cells that are associated with pathogenic conditions such as cancer. One important example is the widespread use of platinum-containing compounds such as cisplatin which damage DNA and induce apoptosis in various cancer cell lines.[7,8] Indeed, the efficacy of cisplatin, carboplatin, and oxaliplatin against testicular and ovarian cancer has sparked significant interest in developing other metal-containing complexes as potential therapeutic agents.[9,10]

Gold(I) complexes (hereafter referred to as Au(I) complexes) are gaining attention for their favorable toxicity toward malignant cells. Over the past five years, there have been several reports of active gold complexes and organometallic derivatives that show cytostatic and/or cytotoxic effects against various cancer cell lines.[11−16] Unfortunately, many of these compounds are nonselective due to the ability of Au(I), a soft Lewis acid, to bind cysteine, selenocysteine, and (less so) histidine residues found in biological systems. One relevant example is auranofin, a glucopyranose containing a triethylphosphine complex of Au(I).[17−22] Auranofin is used as a treatment against rheutamoid arthritis and also produces cytostatic and cytotoxic effects against various cancer cells in vitro.[23−25] Despite these therapeutic uses, however, auranofin causes immunosuppression by inhibiting T-cell proliferation.[22] The mechanism accounting for auranofin's cytotoxicity appears to differ from that of cisplatin as the gold(I) compound does not directly damage DNA.[23−25] Instead, Rigobello et al. demonstrated that auranofin and related Au(I) compounds induce cell death through effects on mitochondrial integrity such as swelling and decreases in mitochondrial membrane potential.[25] These effects are attributed to the inhibition of mitochondrial thioredoxin reductase (TrxR) caused by the binding of Au(I) to the active site selenocysteinate.

One goal of this work was to optimize the therapeutic potential of Au(I)-bearing compounds by encapsulating Au(I) in sterically hindered phosphine ligands to reduce metal ion loss to thiols or selenols in proteins. To this end, we synthesized several indoles substituted with (phosphine)gold(I) fragments at C-5, and we have surveyed their activity as potential anticancer agents. We chose to attach gold covalently to various indolyl-scaffolds because indole is an important bioorganic molecule that serves as a mimic for purines associated with ribose- and deoxyribose nucleos(t)ides.[26] As

Received: May 11, 2011
Published: January 30, 2012

   dx.doi.org/10.1021/jm2005942 | J. Med. Chem. 2012, 55, 2437−2451

such, indole is often used as a key component of various pharmacological agents including staurosporine and indole-3-carbinol.[26−28] Upon the basis of these precedents, we hypothesize that gold-bearing indoles would form ideal candidates to deactivate adenine-binding proteins such as kinases that are often deregulated in cancer.[29] In this respect, tethering Au(I) to indole was predicted to create a surrogate for adenine that would allow delivery of the metal to adenine-binding proteins. The inclusion of a biocompatible gold fragment could expand the chemical space of the simple indole scaffold and produce important pharmacological effects such as increased potency and/or selectivity for a particular target. Alternatively, the inclusion of gold could produce other biological effects through reactions with active site amino acids. Indeed, numerous chemical and biochemical studies indicate that many Au(I) compounds function as prodrugs that undergo specific chemical transformations to generate a pharmacologically active species.[30] These chemical transformations usually consist of fast ligand substitution reactions with rapid aquation in which the resulting cationic species has a strong reactivity with biomolecules. This report demonstrates that (phosphine)Au(I)−indole derivatives act as therapeutic anticancer agents by inhibiting kinases associated with cancer progression rather than inhibiting typical targets such as TrxR.[15,16] In addition, two Au(I) compounds show unique behavior by increasing the cytotoxic effects of ionizing radiation. One compound prevents the cellular detection of double strand DNA breaks (DSBs) by inhibiting the formation of phosphorylated histone H2A (γH2AX) foci after exposure to ionizing radiation. The other (phosphine)Au(I)−indole appears to block steps associated with DSB repair. In either case, the functional outcome is identical, as inhibiting DNA repair leads to an increase in apoptotic cell death. Collectively, the results from these studies provide a novel therapeutic strategy to use Au(I) compounds as radiosensitizing agents against cancer.

RESULTS

Design and Synthesis of Gold(I)−Indoles. The design of (phosphine)Au(I)−indoles unites two themes in medicinal chemistry. The first is the use of indole as a pharmacological scaffold to target specific proteins involved in cancer.[26] The second is the use of gold as a relatively benign metal that can be activated to react with biomolecules, particularly "soft" ligands such as sulfur, selenium, and nitrogen groups present on amino acids such as cysteine, selenocysteine, and histidine. Because several important cellular targets bind indole derivatives, we envision that binding of the Au(I) compound could allow covalent attachment of gold to any of these amino acids that are near the binding site. This reaction could cause irreversible inhibition of important cellular proteins and initiate a biological cascade that leads to eventual cell death by apoptosis (Figure 1A). Indeed, it has been demonstrated that Au(I)-containing compounds can react with enzymes such as TrxR, and that the subsequent inhibitory effects can cause apoptotic effects against various cancer cell lines.[15,16]

Figure 1B summarizes the syntheses of the Au(I)-conjugated indole analogues used in this study. Gold is hardwired to indoles by direct C−Au σ-bonds. Au(I) complexes are predominantly two-coordinate and linear. In the analogues described here, one ligand is an indole (bound through carbon); the other is a capping phosphine. The steric bulk of phosphine ligands can be readily altered. The phosphorus

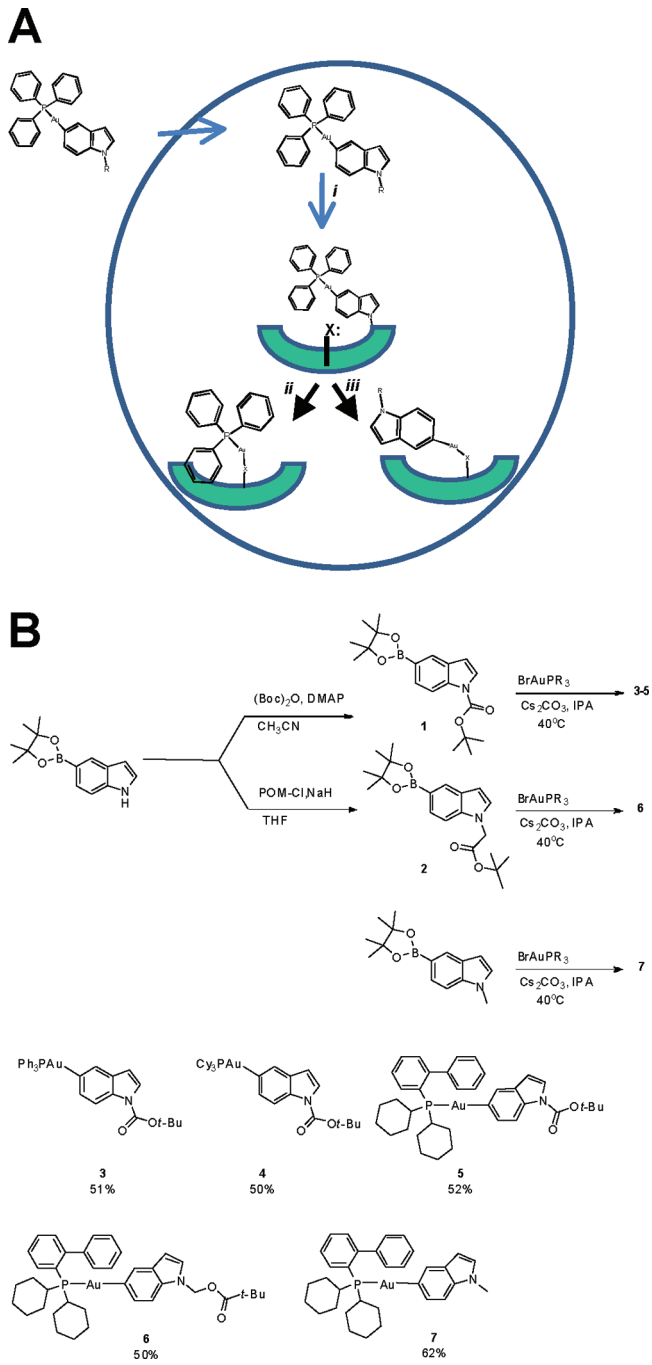

Figure 1. (A) Model describing the potential anticancer effects of (phosphine)gold(I)−indoles. The indole scaffold is a mimic of purine that can interact weakly with ATP-binding proteins, most notably kinases. The inclusion of the phosphine gold(I) ligand can influence the chemical space of this minimal scaffold to increase potency and/or generate selectivity for various targets (i). In addition, the gold molecule can irreversibly react with selected amino acids (cysteine, selenocysteine, and/or histidine) to inactivate potential therapeutic targets (ii and/or iii). In all cases, inhibition of these potential targets can create a variety of downstream effects leading to beneficial cytostatic and/or cytotoxic effects. (B) Synthesis of (phosphine)gold(I)−indoles. See text for complete details.

ligands herein are triphenylphosphine, tricyclohexylphosphine, and a dicyclohexylbiphenylphosphine. Phosphine−gold(I) organometallics were prepared in transmetalation reactions developed by Gray and co-workers.[31−33] Protecting groups

dx.doi.org/10.1021/jm2005942 | J. Med. Chem. 2012, 55, 2437−2451

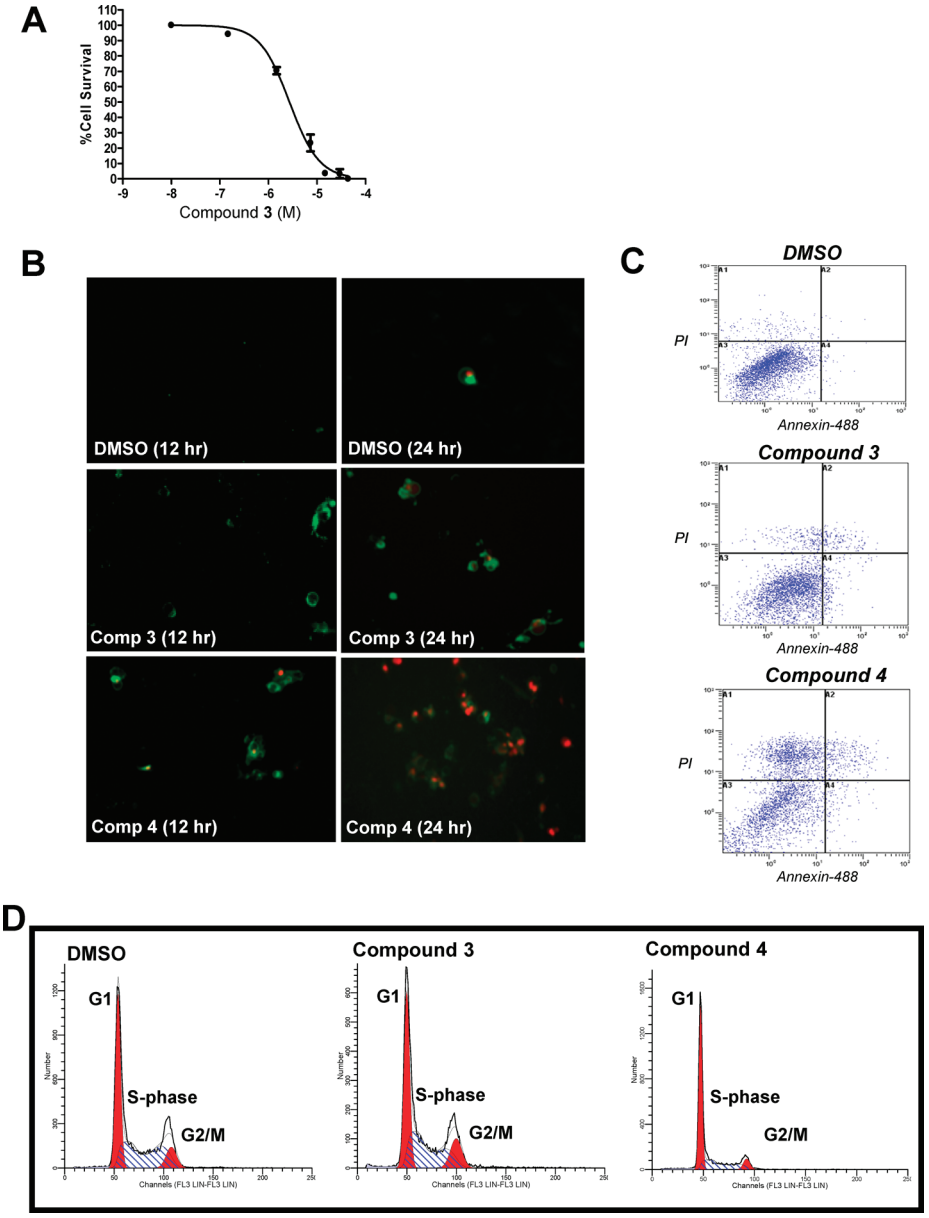

Figure 2. (A) Dose-dependent effects of compound **3** against the adherent cancer cell line, HeLa, demonstrate its anticancer activity. Data were fit to the equation: $y = 100\%/[1 + (IC_{50}/[\mathbf{3}])$ to yield an IC_{50} of 2.5 ± 0.1 μM. (B) Microscopy images using propidium iodide (PI) uptake and annexin V staining in HeLa cells treated with DMSO, 50 μM compound **3**, and 50 μM compound **4** for 12 and 24 h, respectively. (C) Quantitative flow cytometry analyses using propidium iodide (PI) uptake and annexin V staining in HeLa cells treated with DMSO, 50 μM compound **3**, and 50 μM compound **4** after 24 h. (D) Cell cycle analyses of HeLa cells treated with DMSO, 50 μM compound **3**, and 50 μM compound **4** after 24 h.

were added to N1 of indole to prevent coordination at nitrogen. The starting reagent is an indoleboronic acid or pinacol boronate ester. (Phosphine)Au(I) fragments substitute specifically at the boron-bonded carbon; the boron moiety is displaced. Transmetalation proceeds even with bulky phosphorus ligands, such as dicyclohexylbiaryl phosphines.[33] Purity was >95% as judged by high-performance liquid chromatography. In addition, purity of all biologically active compounds was >95% as judged by microcombustion analyses (C, H, N, P, and Au). Details regarding the characterization of each compound using ^{1}H NMR, ^{13}C NMR, ^{31}P NMR, and mass spectroscopy are provided as Supporting Information, as is the crystal structure of compound **3**.

Anticancer Effects of (Phosphine)Au(I)−Indoles. The cellular effects of these (phosphine)Au(I)−indoles were tested against several cancer cell lines including HeLa (cervical cancer), MCF-7 (breast cancer), HCT-116 (colon cancer), and CEM-C7 (leukemia). The dose-dependency of each modified indole on cell viability was assessed using a cell-titer blue assay as previously described.[34] In these experiments, cells were exposed to variable concentrations (0.01−100 μM) of each (phosphine)gold(I)−indole for up to 48 h and then assessed for viability. Representative data provided in Figure 2A shows the dose-dependency of 5-(triphenylphosphine gold(I))−*tert*-butyl 1*H*-indole-1-carboxylate (compound **3**) on HeLa cell viability. These data, representing an average of at least three independent determinations, show that cell viability decreases as the concentration of compound **3** is increased. A fit of the data to eq 1 provides an IC_{50} of 2.5 ± 0.1 μM. This anticancer effect depends upon the presence of the

dx.doi.org/10.1021/jm2005942 | J. Med. Chem. 2012, 55, 2437−2451

Table 1. Summary of IC_{50} Values for (Phosphine)gold(I) Indoles against Adherent and Systemic Cancer Cell Lines[a]

compound	HeLa (μM)	MCF-7 (μM)	HCT116 (μM)	CEM (μM)	selectivity factor[b]
3	2.5 ± 0.1	16.2 ± 0.1	11.5 ± 0.1	19.9 ± 0.1	1.2−8.0
4	16.2 ± 0.1	36.4 ± 0.1	22.8 ± 0.1	9.7 ± 0.1	0.3−0.6
5	2.4 ± 0.1	2.3 ± 0.1	3.4 ± 0.1	2.1 ± 0.1	0.6−0.9
6	0.66 ± 0.05	0.96 ± 0.02	1.8 ± 0.1	0.42 ± 0.10	0.2−0.6
7	0.46 ± 0.01	3.25 ± 0.05	0.38 ± 0.03	1.43 ± 0.05	0.4−3.8

[a]Assay were performed as described in Materials and Methods. IC_{50} values were obtained using a nonlinear regression curve fit of the data to $y = 100\%/[1 + (IC_{50}/\text{inhibitor})]$ where y is the fraction of viable cells, IC_{50} is the concentration of inhibitor that inhibits 50% cell growth, and inhibitor is the concentration of compound tested. All values represent an average of at least three independent determinations performed on different days. [b]Selectivity factor is defined as the ratio of IC_{50} values measured against leukemia cells (CEM-C7) versus adherent cells (SF = $IC_{50\ \text{leukemia}}/IC_{50\ \text{adherent cells}}$). Values greater than 1 indicate that the anticancer effects are more selective for adherent cells compared to the leukemia cell line.

(phosphine)gold(I) ligand, as the nonmetalated indole derivatives do not produce significant anticancer effects even at the highest concentration (100 μM) used.

Identical analyses were performed to measure IC_{50} values for the other (phosphine)Au(I)−indoles, and their values are summarized in Table 1. These data indicate that each compound functions as an independent anticancer agent, displaying potencies ranging from high nanomolar to low micromolar. Despite the presence of a common indole scaffold, however, the potency of each compound is influenced by the nature of the substituent group present at both N1 and C5 of indole. For example, indoles containing electron-donating groups at the N1 position such as compounds **6** and **7** are more potent than compound **5**, which contains an electron-withdrawing group. Likewise, differences in the potencies of structurally similar compounds such as **3** and **4** highlight the pharmacological importance of the phosphine ligand. In particular, the π-electron system within the gold phosphine ligand appears to be important, as the IC_{50} value for compound **3** against adherent cancer cells are at least 2-fold lower than those measured with compound **4** (Table 1).

Another important feature is the unique pharmacological properties of compounds **3** and **4** compared to the other (phosphine)Au(I)−indoles. Specifically, compounds **5**, **6**, and **7** display IC_{50} values that are essentially invariant across the four cancer cell lines tested here. The identity in IC_{50} values suggests that **5**−**7** cause cell death by a nonspecific mechanism, i.e., reacting with one or more macromolecules common to all cell types and that are essential for cellular proliferation or survival. In contrast, the potencies for compounds **3** and **4** vary more significantly across these cell lines. This result suggests that these compounds differentially influence various biological targets present in these diverse types of cancer. In this respect, compound **3** is unique, as it is categorically more potent against all adherent cell lines compared to the leukemia cell line, CEM-C7. The selectivity for compound **3** contrasts that of the structurally related compound **4** which is more efficacious against CEM-C7 cells compared to any of three adherent cell lines tested. (Selectivity is used to describe the observation that compound **3** shows higher potency against adherent cancer cells compared to the leukemia cell line, CEM-C7. This difference argues that this Au(I)−indole could avoid potential side effects such as thrombocytopenia and leukopenia that are caused by inadvertently killing thrombocytes and leukocytes, respectively.) The differences in potency and selectivity for compounds **3** and **4** were deciding factors in further characterizing their anticancer effects alone and in combination with other therapeutic modalities such as ionizing radiation (vide infra).

Cell Death Occurs via Distinct Mechanisms. To further investigate the underlying mechanisms for the effects of compounds **3** and **4**, fluorescence microscopy was used, employing propidium iodide (PI) uptake and annexin V staining as two well established biomarkers of cell death.[35] Figure 2B provides representative microscopy images of HeLa cells treated with DMSO (vehicle) or equimolar concentrations of compound **3** or compound **4** (50 μM). After 12 h, cells treated with either (phosphine)Au(I)−indole show significantly higher levels of annexin V staining compared to cells treated with DMSO and indicates that both Au(I)−indole compounds cause early-stage apoptosis. Furthermore, the lack of significant propidium iodide uptake after 12 h indicates that neither compound induces necrotic cell death at this early time point. However, treatment with compound **4** for 24 h leads to more intense PI staining with a concomitant decrease in annexin V staining. These results suggest that cells transit from early- to late-stage apoptosis within 12 h. In contrast, significant PI uptake is not observed in cells treated with compound **3**, even after 24 h. Instead, a steady increase in the amount of annexin V staining is observed over the 24 h time period.

Dual parameter FACS analyses with PI and annexin V staining was next performed to quantify these differences and shed more insight into the mechanism of cell death. Representative data averaged over three independent determinations are provided in Figure 2C. These data show that treatment with compound **3** for 24 h produces significantly higher amounts of early- and late-stage apoptosis compared to cells treated with DMSO. As summarized in Table 2, compound **3** causes a 6-fold increase in early-stage apoptosis and a ∼10-fold increase in late-stage apoptosis compared to treatment with DMSO. In addition, the lack of PI uptake again supports the conclusion that compound **3** does not cause necrosis.

Table 2. Summary of the Effects of Treating HeLa Cells with (Phosphine)gold(I)−Indoles

compound	live (%)	early apoptotic (%)	late apoptotic (%)	necrotic (%)
DMSO	94.8 ± 0.6	1.5 ± 0.1	0.10 ± 0.02	3.6 ± 0.4
3[a]	84.4 ± 3.0	8.8 ± 0.7	4.3 ± 1.8	2.4 ± 0.8
4[b]	68.4 ± 0.8	5.3 ± 1.1	8.1 ± 1.8	18.8 ± 2.5

[a]A concentration of 50 μM was used which is 20-fold higher than the IC_{50} value reported in Table 1. All values represent an average of at least three independent determinations performed on different days. [b]A concentration of 50 μM was used which is 3-fold higher that the IC_{50} value reported in Table 1. All values represent an average of at least three independent determinations performed on different days.

dx.doi.org/10.1021/jm2005942 | J. Med. Chem. 2012, 55, 2437−2451

Several important differences are noted in HeLa cells treated with compound **4**. One distinction is that lower amounts of early-stage apoptosis are detected with compound **4** compared to compound **3** (5.3% versus 8.8%, respectively). In addition, compound **4** generates a 2-fold higher amount of late-stage apoptotic cells compared to compound **3** (8.1% versus 4.3%, respectively). However, the most striking difference is that compound **4** causes necrotic cell death as evidenced by extensive PI uptake in the absence of appreciable annexin V staining. Quantitative analysis reveals that treatment with compound **4** causes a ~9-fold higher amount of necrosis compared to treatment compound **3**. Collectively, the differences in the mechanism and timing of cell death upon treatment with compounds **3** versus **4** highlight how subtle differences in the structure of the Au(I)−ligand can produce significant pharmacological effects.

We next analyzed the effects of compounds **3** and **4** on cell-cycle progression after 24 h post-treatment using PI staining to measure cellular DNA content. Figure 2D provides a histogram of HeLa cells treated with DMSO. This represents a standard cell-cycle distribution for asynchronous cells, as the vast majority of cells exist at G1 (45.6 ± 0.1%) and S-phase (43.6 ±0.1%) while a significantly smaller population exists at G2/M (10.8 ± 0.1%). Treatment with compound **3** does not cause any significant alterations in cell-cycle progression over a 24 h period (Table 3). Thus, compound **3** induces apoptosis without overtly perturbing cell-cycle progression. A different phenomenon is observed after treating the cells with compound **4** due to the significant accumulation at G1 (60.3 ± 3.2%) with a concomitant decrease at S-phase (28.3 ± 1.3%) (Table 3). These combined effects indicate that compound **4** blocks cellular entry into S-phase. However, this blockade evokes more of a necrotic form of cell death as opposed to a classic apoptotic response. Regardless, these data again highlight the ability of structurally related Au(I) compounds to produce different effects on cell-cycle progression.

Table 3. Summary of the Effects on Cell-Cycle Progression by (Phosphine)gold(I)−Indoles[a]

compound	G1 (%)	S-phase (%)	G2/M (%)
DMSO	45.6 ± 0.1	43.6 ± 0.1	10.8 ± 0.1
3[b]	45.4 ± 2.1	41.6 ± 0.1	13.0 ± 2.1
4[c]	60.3 ± 0.8	28.3 ± 1.3	11.4 ± 4.9

[a]HeLa cells were used in these experiments. Cells were analyzed 24 h post-treatment. All values represent an average of at least three independent determinations performed on different days. [b]The concentration of 50 μM used in this experiment is 20-fold higher than its IC_{50} value. [c]The concentration of 50 μM is 3-fold higher than its IC_{50} value

These effects prompted us to evaluate the cytotoxicity of the unprotected gold(I) complex, $BrAuPPh_3$. When tested against the leukemia cell line, CEM-C7, this unprotected Au(I) complex displayed potent cytostatic and cytotoxic effects (Supporting Information, Figure S26). The dose-dependency of $BrAuPPh_3$ in generating a cytotoxic effect yielded an LD_{50} of 0.22 ± 0.05 μM, a value which is ~40−80-fold lower than that measured for compound **3** or **4**. Despite this higher potency, treatment of CEM-C7 cells with $BrAuPPh_3$ causes necrosis as evidenced by significant uptake in propidium iodide (A. Berdis, unpublished results). This distinction is important, as it indicates that encapsulating Au(I) with sterically hindered phosphine ligands reduces its ability to nonselectively react with biological targets to cause necrosis. Defining this mechanism of cell death is important, as necrosis can cause various side-effects including septic shock and kidney failure that can obviously compromise patient health. Surprisingly, the unprotected Au(I)−phosphine ligand, $BrAuPPh_3$, does not produce significant cytostatic or cytotoxic effects against the adherent cell line, HeLa, up to a concentration of 100 μM (Supporting Information, Figure S27). As such, the protected Au(I)−indoles have significantly higher potencies against adherent cells. The dichotomy in the potency of $BrAuPPh_3$ against the leukemia cell line versus adherent cells is not clear at this time. However, likely possibilities include nonselective reactions between cellular proteins and the unprotected $BrAuPPh_3$ and/or inhibition of thiol-and selenocysteine-containing enzymes such as TrxR that is involved in maintaining nucleoside homeostasis (vide infra).

Reactivity of Au(I) Compounds toward Biological Thiols. The most abundant plasma protein and principal extracellular source of sulfhydryl groups is serum albumin. This protein plays important roles by transporting numerous compounds including metals, amino acids, hormones, fatty acids, and medicinal drugs. Although serum albumin contains 35 cysteines, all but one exist as disulfide bonds. Cys34 is the only residue in serum albumin that can exist as a reduced thiol or as a mixed disulfide of cysteine or glutathione. The pK_a of Cys34 is approximately 5.0 and thus more acidic than cysteine or glutathione, which have pK_as of 8.5 and 8.9, respectively. Collectively, the biological abundance and lower pK_a value of Cys34 predicts that it is highly reactive toward Au(I) and would favor exchange reactions with Au(I)-containing complexes.[36]

We tested the ability of various Au(I) complexes to nonselectively react with BSA using modifications to protocols established by Shaw et al.[37] and Roberts et al.[38] In a typical experiment, variable concentrations of BSA (0−120 μM) were treated with a fixed concentration of compound **3** (120 μM) or compound **4** (120 μM), yielding Au(I)/BSA ratios of 4:1, 2:1, 1:1, and 0:1. After an incubation for 1 h, the reaction mixtures were applied to Penefsky spun columns using P2 gel filtration resin and centrifugal force to rapidly and efficiently separate unreacted Au(I)-containing complexes from BSA. P2 resin was effective in retaining Au(I)-containing compounds including compound **3** and compound **4**. However, BSA was not retained in the resin as >95% of the BSA loaded into the Penefsky column is recovered in the eluant. After recovery from the column, the SH titer of BSA was determined using DTNB as previously described for reactions performed at varying concentrations of Au(I)−indole. Values obtained from reactions containing BSA incubated with the various Au(I) complexes were compared to identical reactions containing BSA alone and eluted through Penefsky columns. Data provided as Supporting Information (Figure S28) show that the relative thiol content of BSA remains unchanged in the presence of compound **3**, even at the highest Au(I)/BSA ratio of 4:1. Identical experiments performed with compound **4** yield similar results (Supporting Information, Figure S29). Positive control experiments measured the reactivity of $BrAuPPh_3$ with BSA and demonstrated facile interactions of the unprotected Au(I)−ligand with the reactive cysteine residue present on BSA (Supporting Information, Figure S30).

To further interrogate the stability of these Au(I) complexes, we next measured the reactivity of compounds **3** and **4** toward L-cysteine. In this case, the SH content of variable

dx.doi.org/10.1021/jm2005942 | J. Med. Chem. 2012, 55, 2437−2451

concentrations of cysteine was determined using DTNB as described above. Varying the concentration of L-cysteine generates a linear standard curve (Supporting Information, Figure S31). Compound **3** alone gives an absorbance reading equivalent to background, indicating that the Au(I)−indole does not react with DTNB. Incubation of 400 μM L-cysteine with an equivalent concentration of compound **3** does not cause a change in the amount of free SH present on L-cysteine. If L-cysteine had reacted with Au(I) present on compound **3**, then a decrease in the amount of free or unligated SH on L-cysteine would have been observed. The identity in A_{412} for L-cysteine in the absence and presence of compound **3** provides additional evidence for the lack of a displacement reaction by biological thiol groups.

Inhibitory Effects against Thioredoxin Reductase. The inhibitory effects of compound **3**, compound **4**, and the unprotected Au(I)−phosphine ligands ($BrAuPPh_3$ and $BrAuPCy_3$) were measured against rat liver TrxR. The activity of TrxR was measured using a standard DTNB assay as previously described.[39] In this assay, TrxR uses DTNB as a substrate to generate two molecules of 5′-thionitrobenzoic acid (TNB) with the concomitant generation of $NADP^+$ from NADPH and H^+. Time courses in product formation are generated as increases in the absorbance at 412 nm due to the generation of 2 equiv of TNB from the reduction of DTNB. Figure 3 provides representative time courses in TrxR activity

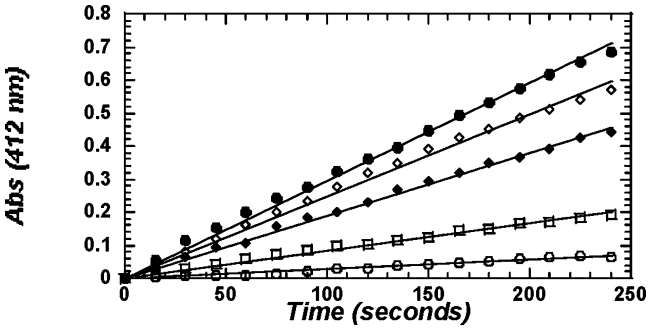

Figure 3. Inhibition of thioredoxin reductase activity by Au(I)−indoles. Experiments were performed by adding 600 nM TrxR to a preincubated solution containing 100 mM potassium phosphate, pH 7.0, 10 mM EDTA, 5 mM DTNB, 0.2 mg/mL BSA, 240 μM NADPH in the absence (●) or presence of 40 μM compound **3** (◇), 40 μM compound **4** (◆), or 1 μM $BrAuPPh_3$ (□). The background rate in DTNB reduction (○) was determined by performing identical reactions in the absence of TrxR and Au(I)-containing compound.

in the absence and presence of compound **3**, compound **4**, and the unprotected Au(I)−phosphine complex, $BrAuPPh_3$. Each time course represents an average of three independent determinations. The unprotected Au(I)−phosphine complex, $BrAuPPh_3$, inhibits 85% of TrxR activity at a low concentration of 1 μM. This result indicates that $BrAuPPh_3$ causes nearly 100% inhibition at stoichiometric levels of TrxR. The ability of $BrAuPPh_3$ to inhibit TrxR activity highlights the ability of unprotected gold compounds to undergo facile reaction with selenoenzymes. In contrast, both compounds **3** and **4** are poor inhibitors of TrxR activity. Specifically, compound **3** inhibits 17% TrxR activity at a fixed concentration of 40 μM while compound **4** inhibits 39% of TrxR activity at an equivalent concentration. Although the Au(I)−indoles can affect TrxR activity, it should be noted that this low level of inhibition occurs at a concentration of 40 μM which is significantly higher than the IC_{50} values for either compound measured using the viability assay (vide supra). These results, coupled with the results of experiments validating the stability of both compounds **3** and **4**, collectively indicate that these gold-containing indoles do not cause cellular effects by reacting with thiol- or selenol-containing proteins like TrxR.

Screening for Kinase Inhibition. Since neither compound **3** or **4** displays appreciable inhibitory effects against known cellular targets of gold such as TrxR, we next tested for inhibitor effects against adenine-binding proteins including kinases. It is well established that dysfunctional and unregulated kinase activity plays significant roles in cancer initiation and progression.[29] Both compounds **3** and **4** were profiled against a panel of 64 kinases using a commercially available screening assay to evaluate if the measurable differences in cell-cycle progression and cell death arise from inhibitory effects on any of these cellular targets.[40] Experiments were performed using protocols described by Luceome Biotechnologies (Tucson, AZ), maintaining the concentration of compounds **3** and **4** fixed at 10 μM. Table 4 provides a report of the percentage inhibition exhibited by compound **3** and **4** as a function of these representative human kinases. Inspection of the data provides several interesting observations. First, it is clear that neither compound **3** or **4** exhibits high potency toward any of the kinases present in this library. Despite the low potencies, however, a small number of kinases are inhibited by ∼40% when the concentration of either compound **3** or **4** are maintained at 10 μM. These inhibitory effects at this concentration are consistent with their measured IC_{50} values that are also in the micromolar range (Table 1). In addition, several kinases display overlapping inhibitory responses to both Au(I) compounds. Many of these are of particular interest due to their involvement in cancer initiation and/or progression. For example, the Aurora kinase family members, Aurora A and Aurora B, as well as the MARK2 and MARK3 kinases, function during mitosis to regulate cell division.[41,42] These kinases are important therapeutic targets, as their activities are often deregulated in many types of cancers.[43] Other kinases such as RPS6KA3 and MLK3 are involved in the MAP kinase and JNK pathways which are also important in cancer progression.[44−46] Thus, despite the low potency of Au(I) compounds, the ability to weakly inhibit multiple therapeutic targets provides a plausible mechanism to explain their anticancer effects. Indeed, several recent reports have established a new treatment paradigm for using compounds that display low potencies toward inhibiting multiple targets associated with a cancer phenotype.[47−49] It is argued that using a single, less-specific drug to inhibit various cellular targets may have therapeutic benefits compared to multidrug regimens that produce similar outcomes.

While compounds **3** and **4** display some overlap in inhibitory effects, compound **4** is a more promiscuous kinase inhibitor compared to compound **3**. In this respect, only six kinases show greater than 20% inhibition with 10 μM of compound **3** while an equivalent concentration of compound **4** inhibits 18 kinases to the same extent. The ability of compound **4** to inhibit certain kinases such as SNF1LK, YES1, and SNARK is noteworthy, as they are involved in various pathological conditions. For example, YES1 is proto-oncogene that plays a role in cancer metastasis by functioning as a tyrosine protein kinase.[50] SNARK is another potential anticancer target, as this kinase, normally involved in regulating glucose metabolism, may fuel carcinogenesis.[51] In general, the ability of compound **4** to

Table 4. Summary of the Inhibitory Effects of (Phosphine)gold(I)−Indoles on a Panel of Various Human Kinases[a]

kinase	compound 3 (% inhibition)	compound 4 (% inhibition)	kinase	compound 3 (% inhibition)	compound 4 (% inhibition)
AKT1	0	0	MARK3	6.5	34
AKT2	25.8	33.6	MET	15.1	23.3
AKT3	0	0	MLK1	32.5	42.2
AMPK-α1	0	0	MLK3	31.2	43
AMPK-α2	0	0	MST2	0	0
AURKA	26.7	41.7	P38-γ	0	0
AURKB	11.1	24.5	PAK1	0	0
AURKC	23.9	35.0	PDGFRB	8.1	15.2
BLK	0	0	PDK1	17.4	24.3
CAMK1	0	0	PIM1	0	10.6
CAMK1D	0	0	PIM2	0	8.7
CAMK1G	0	0	PKAC-α	0	12.4
CAMK2B	0	0	PKC-ε	0	5.9
CAMK2D	0	0	PKC-δ	0	3.8
CAMKK1	0	0	PKC-η	3.2	0
CAMKK2	0	7.9	PRKD2	0	3.8
CHEK1	0	0	PKG1	5.4	3.2
CLK1	0	0	RPS6KA1	0	0
CLK2	0	0	RPS6KA3	16.7	34.9
DDR2	0	0	RPS6KA4	1.0	21.8
FGFR2	0	0	RPS6KA5	0	5.0
FLT1	0	9.4	SNF1LK	0	40.6
FLT2	0	0	SNF1LK2	0	32.9
FLT3	0	0	SLK	0	19.6
FYN	0	1.2	SNARK	0	39.5
GSK3α	0	5.8	SRC	14.3	5.2
IGF1R	0	4.7	SYK	21.6	40.7
ITK	0	3.1	TNK2	0	2.2
LYN	0	0	VEGFR2	0	5.8
MARK1	5.1	11.9	YES1	0	31.7
MARK2	18.9	26.2	YSK1	0	20.9

[a]The concentration of compounds 3 and 4 were maintained fixed at 10 μM. Assays were performed as described.[40]

inhibit these kinases provides a new strategy to generate selective modulators of these therapeutic targets.

Enhancing the Cytotoxicity of Ionizing Radiation via (Phosphine)gold(I)−Indoles. Because compounds **3** and **4** inhibit kinases associated with cancer progression, we next tested their ability to enhance the anticancer effects of existing therapeutic modalities. In this case, we measured the effects of combining these (phosphine)Au(I)−indoles with ionizing radiation (IR), a widely used therapy used to treat solid tumors. Experiments were performed by pretreating HeLa cells with compounds **3** or **4**, using sublethal concentrations, i.e., concentrations that produce <10% cell death over a 24 h period. After this time frame, medium containing the (phosphine)Au(I)−indole was removed and replaced with fresh medium. The cells were then irradiated in a dose-dependent fashion from 0 to 6 Gy. Cell viability was assessed using a clonogenic assay that measures colony formation and thus accurately defines the cytotoxic effects of IR exposure.[52] Figure 4A shows the relationship between radiation dose with the fraction of cells that survive exposure to these doses of IR. HeLa cells treated with IR alone show a typical linear-quadratic survival curve characterized by an initial linear cell killing phase that is proportional to the dose of radiation followed by a second cell killing phase that is proportional to the square of the dose. The initial linear phase is particularly important, as this reflects the ability of the cell to repair damaged DNA inflicted by clinically relevant doses of IR (~2 Gy). This initial phase is eliminated when cells are pretreated with compound **3** (4 μM) or compound **4** (7 μM) (Figure 4A). The ability of either compound **3** or **4** to increase the slope of this initial phase provides clear evidence that both Au(I)-containing compounds enhance the cell killing activity of IR. In fact, the radiosensitizating effect exhibited by these compounds is reminscent of survival curves generated in cells defective in kinases involved in repairing DNA damage such as ataxia telangiectasia mutated (ATM) and ataxia telangiectasia and Rad-3 related (ATR).[53,54] Quantitative analyses reveal that cells treated with either compound **3** or **4** are ~4-fold more sensitive to the effects of IR exposure than cells treated with IR alone. Compounds **6** and **7** do not enhance the cell killing effects of IR. This dichotomy implies that compounds **3** and **4** exert their effect by binding selective cellular proteins including kinases while the nonspecific analogues **6** and **7** do not.

The underlying mechanism for these radiosensitizing effects was further interrogated by quantifying the number of DSBs formed after IR exposure in the absence and presence of compounds **3** and **4** using γH2AX as a biochemical marker (Figure 4B).[55] Histograms provided in Figure 3C−H show plots of the percentage of cells containing γH2AX foci after exposure to 2 Gy IR after 30 min or 4 h, respectively. Cells treated with DMSO show an increased number of γH2AX foci 30 min post-IR exposure (Figure 4C). This rapid response is indicative of DSB formation via radical damage.[56] The vast majority of these DSBs are repaired within 4 h as judged by

dx.doi.org/10.1021/jm2005942 | J. Med. Chem. 2012, 55, 2437−2451

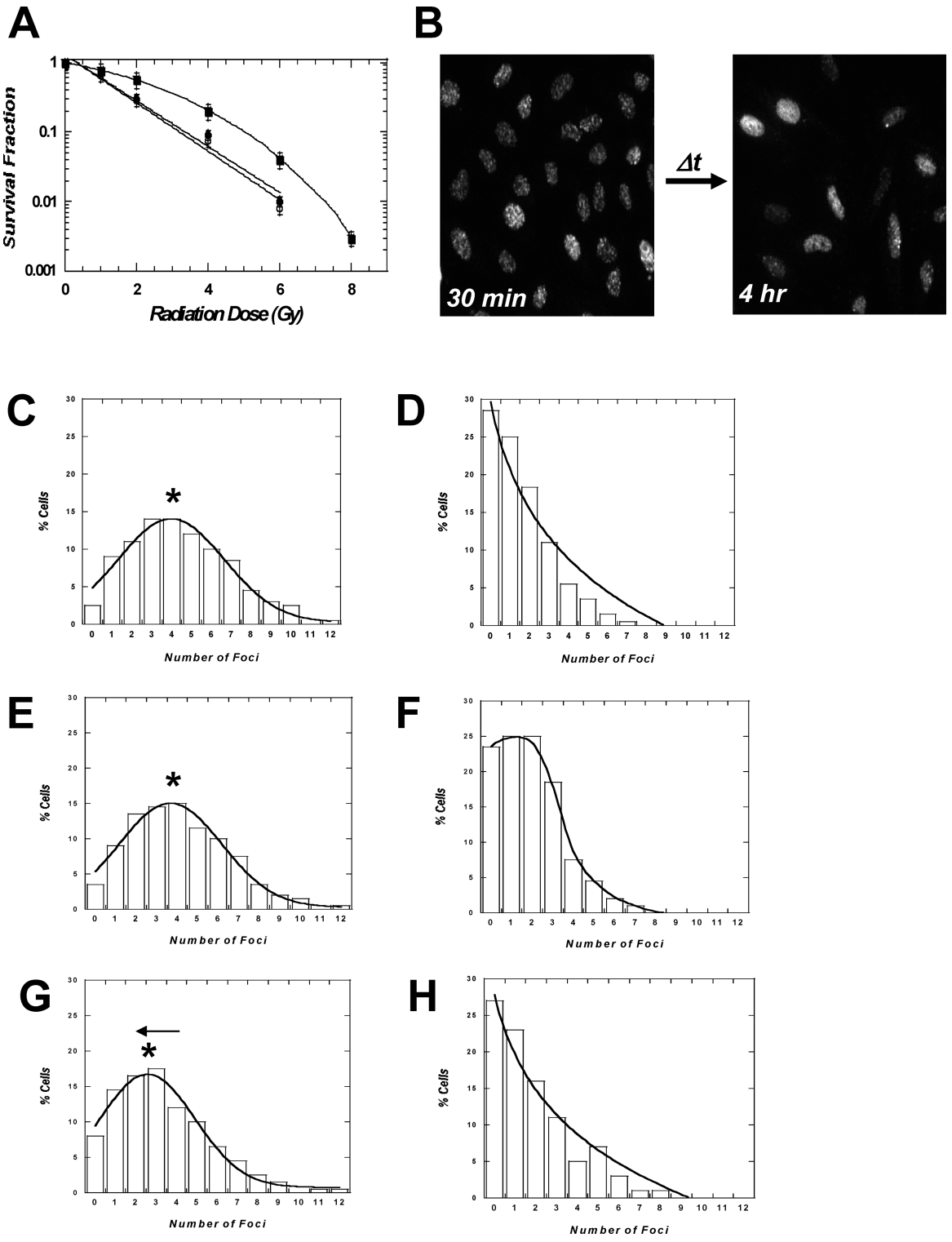

Figure 4. (A) Plot of the survival fraction versus dose of IR exposure for HeLa cells in the absence (■) or presence of 4 μM compound **3** (●) or 7 μM compound **4** (○). (B) γH2AX foci formation for HeLa cells treated with DMSO and 2 Gy IR after 30 min (left panel) or 4 h (right panel). Histograms for HeLa cells treated with 2 Gy of IR under the following conditions: (C) DMSO, 30 min post-IR exposure; (D) DMSO, 4 h post-IR exposure; (E) compound **4** (7 μM), 30 min post-IR exposure; (F) compound **4** (7 μM), 4 h post-IR exposure; (G) compound **3** (4 μM), 30 min post-IR exposure; (H) compound **3** (4 μM), 4 h post-IR exposure.

fewer γH2AX foci (Figure 4D). HeLa cells treated with compound **4** also show an increase in the number of γH2AX foci 30 min post IR exposure (Figure 4E). However, a significant number of γH2AX foci persist 4 h after IR exposure in cells pretreated with compound **4** (Figure 4F). The attenuation in γH2AX foci disappearance indicates that compound **4** inhibits DSB repair, and this inhibition likely accounts for the enhancement in IR cytotoxicity caused by this gold-containing indole.

dx.doi.org/10.1021/jm2005942 | J. Med. Chem. 2012, 55, 2437–2451

A different effect on γH2AX foci formation is observed combining compound **3** with 2 Gy of IR. As illustrated in Figure 4G, cells pretreated with compound **3** have fewer γH2AX foci 30 min after IR exposure compared to cells treated with either DMSO or compound **4**. This reduction in γH2AX foci formation suggests that compound **3** inhibits H2AX phosphorylation without influencing the overall number of DSBs formed after IR exposure. The ability of compound **3** to prevent phosphorylation is reasonable, as we have shown that this Au(I)−indole inhibits the activity of several kinases (Table 4). Indeed, phosphorylation of H2AX is catalyzed by several PI3K-like kinases including ATM, ATR, and DNA-dependent protein kinase (DNA-PK).[37] After DSB formation, each kinase is rapidly activated, and their ability to phosphorylate key proteins such as H2AX is essential for the timely repair of these lesions.[44] While we do not know if any of these specific kinases are influenced by compound **3**, it is tempting to speculate that they are either directly or indirectly inhibited by this gold compound. Current efforts are exploring this possibility. Regardless, the net effect for inhibiting H2AX phosphorylation is a reduction in DSB repair that causes a concomitant increase in the cytotoxic effects of IR observed in our clonogenic assays.

DISCUSSION

This report describes the development and application of unique (phosphine)gold(I)−indoles that function as anticancer agents when used individually and in combination with therapeutic doses of IR. The anticancer activity of these compounds is not unprecedented as several Au(I) and Au(III) complexes have been reported to generate favorable anticancer effects.[11−16,25] One of the most relevant cellular targets for many gold compounds is TrxR, the only known enzyme that catalyzes the reduction of thioredoxin.[58] Thioredoxin plays important roles ranging from maintaining nucleotide pools associated with DNA replication and repair to defending against oxidative stress directly and indirectly via redox signaling.[58] As such, inhibiting TrxR activity can produce robust anticancer effects. For example, Rubbiani et al. reported that Au(I) complexes with benzimidazole-derived N-heterocyclic carbene ligands displayed more potent inhibition against TrxR compared to the closely related redox enzyme, glutathione reductase.[11] In this case, the selective inhibition of TrX activity coincided with significant cytostatic effects against various cancer cell lines. In addition, Yan et al. reported that Au(I)-containing N,N′-disubstituted cyclic thiourea complexes inhibit TrxR with nanomolar potencies.[12] As expected, several of these compounds also exerted significant cytotoxic effects against cancer cells presumably as a result of this inhibition. Another recent example comes from the work of Vergara et al., demonstrating that Au(I) complexes containing phosphine ligands such as 1,3,5-triaza-7-phosphaadamantane and 3,7-diacetyl-1,3,7-triaza-5-phosphabicyclo[3.3.1] attached to thionate ligands show cytostatic effects against cisplatin-sensitive (A2780S) and -resistant (A2780R) ovarian cancer cells.[13] Similar to results published by Rubbiani et al., these Au(I)−phosphine complexes inhibited both cytosolic and mitochondrial TrxRs while being relatively inert against the related glutathione reductase. Finally, Maiore et al. recently published on the synthesis and biological characterization of Au(I) and Au(III) complexes based on the saccharinate ligand.[14] In general, Au(III) complexes displayed moderate cytotoxicities against the A2780S ovarian cancer cell line while only modest activities were observed with disaccharinato gold(I) complexes. The higher reactivity of Au(III) saccharinate derivatives compared to the Au(I) counterparts correlate with their increased cytotoxic effects.

While TrxR is an excellent target for many Au(I)-containing complexes, other cellular enzymes can be efficiently inhibited by related gold complexes. For example, Zhang et al. demonstrated that Au(I)−dithiocarbamato species show inhibitory effects against another therapeutic target, i.e., the proteolytic activity of 20S proteasome and 26S proteasome in human cancers.[15] Inhibiting the proteasome caused the accumulation of ubiquitinated proteins and proteasome target proteins and ultimately caused cell death. Likewise, Trani et al. showed that aurothiomalate, a gold compound similar to auranofin that is used to treat rheumatoid arthritis, shows unique pro-apoptotic effects in cancer cells via the disruption of the PKCiota-Par6 complex.[16] Disruption of this complex leads to the activation of the ERK pathway, causing caspase-3 activation and subsequent apoptosis. In addition, aurothiomalate activates the p38 and JNK MAP kinases. Finally, Bagowski et al. demonstrated that Au(I)−phosphine complexes containing a naphthalimide ligand display antiangiogenic effects in two different zebrafish angiogenesis models, including a tumor-cell-induced neovascularization assay.[59] While the exact cellular target responsible for this anticancer effect has yet to be conclusively identified, the beneficial therapeutic effect is unlikely to be related to TrxR inhibition. Collectively, these studies highlight the ability of gold complexes to exert cytotoxic effects by inhibiting cellular targets other than TrxR.

In this report, we describe two Au(I)−indoles that show unique properties by killing cancer cells without adversely affecting TrxR activity. This ability contrasts that of the unprotected Au(I)−ligand, $BrAuPPh_3$, which produces potent cytotoxic effects in leukemia cells by inhibiting TrxR activity. As such, the low reactivity displayed by compounds **3** and **4** against BSA or inhibiting TrxR activity is consistent with our original hypothesis that encapsulating Au(I) with sterically hindered phosphine ligands reduces the reactivity of this metal with biological thiols or selenols. This result is also consistent with structure−activity relationships reported by Shaw et al. showing that the ease of displacing trialkylphosphines from their albumin−gold complexes to be $Me_3P > Et_3P > i\text{-}Pr_3P$.[37] As such, using bulky ligands such as triphenylphosphine or tricyclohexylphosphine reduces reactivity toward thiol groups. In addition, the potencies of compounds **3** and **4** vary among the cancer cell lines tested here, suggesting that they inhibit selective molecular targets within the cell. Screening of both Au(I) compounds against a panel of human kinases provides evidence that for their inhibitory effects against several potential therapeutic targets. The data provided in Table 4 indicates that the structurally related compounds inhibit some common kinases with different potencies. In particular, compound **4** shows a higher degree of promiscuity by interacting with three-times as many kinases compared to compound **3**. The combination of variable potencies and promiscuity for inhibiting different targets provides a reasonable explanation for the nuances observed in their physiological effects. We emphasize that these screening efforts cover ∼10% of the reported 520 different protein and lipid kinases that constitute the human kinome. As such, it is likely that these Au(I)−indoles also inhibit other therapeutically relevant kinases not present in this initial screen. In fact, the ability of compound **4** to inhibit G1- to S-phase progression suggests that this gold compound inhibits other kinases including cyclin-dependent

dx.doi.org/10.1021/jm2005942 | J. Med. Chem. 2012, 55, 2437−2451

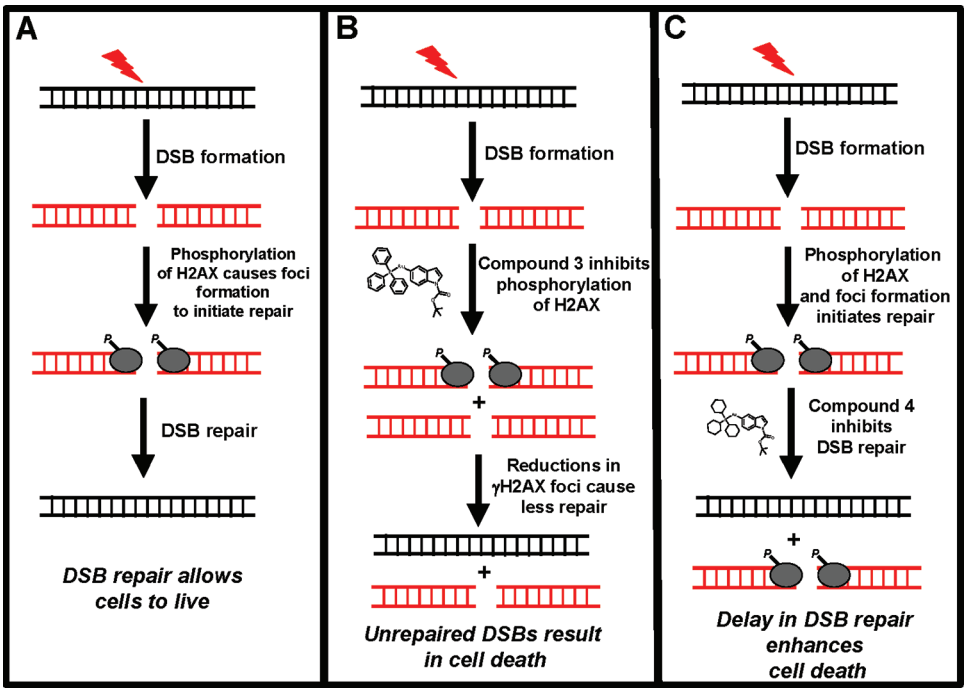

Figure 5. Proposed models for the enhancement of IR-induced cytotoxicity by compounds **3** and **4**. (A) Under normal conditions, exposure to IR induces DNA damage that can be repaired through activation of ATM, ATR, and DNS-PK. (B) Compound **3** inhibits DNA repair by directly or indirectly blocking the phosphorylation of H2AX. Reductions in γH2AX foci formation leads to a reduction in DNA repair. (C) Compound **4** inhibits the repair of DSBs through mechanisms independent of γH2AX foci formation. See text for further details.

kinases (cdks 2, 4, and 6) that are involved in cell-cycle progression.[60] Current efforts are exploring these possibilities.

Another important feature of this work is that these Au(I)−indoles potentiate the cytotoxic effects of IR exposure at concentrations that are fractions of their respective LD_{50} values. IR is an important therapeutic modality used in approximately one-half of all cancer patients and is particularly effective against cancers of the brain, cervix, breast, and colon that are inaccessible to surgery and/or refractory to chemotherapy.[61−64] Although the primary target of therapeutic IR is water in tissue, the radicals derived from water eventually damage DNA. While IR produces several forms of DNA damage, the most lethal are double-stranded DNA breaks (DSBs).[65] In general, the inability of a cancer cell to effectively repair these DSBs causes both cytostatic and cytotoxic effects to reduce tumor growth.

IR is relatively effective in amply oxygenated tissue, and this reflects the ability of long-lived oxygen-centered radicals to be more effectively propagated to DNA.[66] Unfortunately, the inner volumes of many solid tumors are hypoxic and cause radiation-resistant zones.[67] As such, a major complication in IR therapies is effectively killing radiation-resistant cells. Approaches to improve the efficacy of IR have focused on using DNA-damaging agents such as cisplatin to enhance cell death by overwhelming DNA repair pathways.[68] Alternatively, antimetabolites such as 5-fluorouracil can be used to reduce intracellular dNTP pools needed to resynthesize DNA during repair.[69,70] While these approaches work, these specific chemotherapeutic agents are themselves highly cytotoxic and thus kill both cancerous and healthy cells.[71] Indeed, the nonselective killing of healthy, normal cells produces severe side effects including anemia, leukopenia, and thrombocytopenia that are significant complications in effectively treating patients. The results described here with our Au(I)-containing compounds provide an alternative approach to potentiate the cytotoxic effects of IR.

Our data show that compounds **3** and **4** function as radiosensitizers to inhibit DSB repair through two mutually exclusive mechanisms. As illustrated in Figure 5A, exposure to IR produces DSBs that cause the phosphorylation of H2AX. This acts as a key signaling event that initiates DSB repair which allows cells to survive the insult to genomic DNA. Compound **3** inhibits H2AX phosphorylation, leading to a decrease in γH2AX foci formation (Figure 5B). By blocking this key step, compound **3** causes a significant number of DSBs to be left unrepaired to enhance the extent of apoptosis. The structurally related analogue, compound **4**, also inhibits DSB repair and increases the cytotoxicity of IR. However, compound **4** does this via a different mechanism that involves the inhibition of steps occurring after γH2AX foci formation (Figure 5C). It is tempting to speculate that the potentiating effect caused by compound **4** reflects inhibition of cell-cycle progression. However, more data are needed to prove this hypothesis.

Regardless, we envision that the potentiating effect by either Au(I) compound is caused by reversible inhibition of key cellular proteins such as kinases involved in DNA repair and/or cell-cycle progression. This argument is strengthened by the observation that other (phosphine)gold(I)−indoles including compounds **6** and **7** do not enhance the cell killing effects of IR (data not shown). This dichotomy implies that compounds **3** and **4** exert their effect by binding selective cellular proteins while the nonspecific analogues, **6** and **7**, do not. Another possible mechanism is that IR exposure leads to radical induced cleavage of the Au(I)-containing indole which then inflicts irreversible damage on these cellular components. This prediction is based upon the results of density-functional theory calculations for these gold-bearing compounds. As illustrated in Figure 6, the dissociation energy of the gold−carbon bond into radicals is approximately 58 kcal mol^{-1} while

dx.doi.org/10.1021/jm2005942 | J. Med. Chem. 2012, 55, 2437−2451

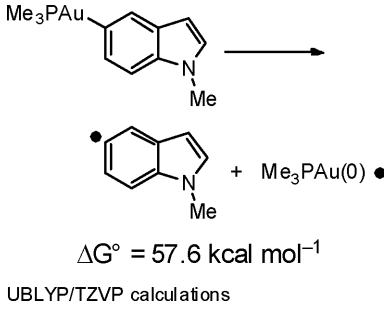

Figure 6. Homolytic bond dissociation energy of a model Au(I)–indole. See text for details.

the experimental dissociation energy of HO–H is 119 kcal mol^{-1}.[72] Because metal–carbon bonds are weaker than the O–H bond of water, it is possible that radicals initiated by IR are transduced from water radicals to these Au(I) compounds to produce gold or carbon radicals. If so, then Au(I) organometallics containing homolyzable carbon–gold bonds have therapeutic prospects by potentiating damage caused by radicals brought about by IR or other radical-generating systems.

Finally, while both (phosphine)gold(I)–indoles increase the cytotoxic effects of IR, compound **3** may prove to be more efficacious than compound **4**. This is based on the fact that compound **3** shows higher potency against adherent cancer cells compared to the hematological cancer cell line, CEM-C7. The lower potency against systemic cancer cells implies that this novel gold–indole analogue could avoid potential side effects such as thrombocytopenia and leukopenia that are caused by inadvertently killing thrombocytes and leukocytes, respectively. This selectivity combined with the measured dose-modifying factor of 4 indicates that this (phosphine)Au(I)–indole could be used to increase the effectiveness of ionizing radiation, especially for clinical protocols that require fractionation of large IR doses. By increasing the efficacy of IR, these innovative gold-bearing indoles can be used to reduce total exposure to ionizing radiation. This will provide additional therapeutic benefits by lowering the risk of developing complications associated with excessive exposure to ionizing radiation that include side effects such as inflammation, gastrointestinal ailments, and immunosuppression. Current efforts are further exploring the therapeutic utility of these and other gold-bearing indole derivatives.

MATERIALS AND METHODS

Reagents and General Methods. Acetonitrile (Acros Organics) was distilled from CaH_2. Tetrahydrofuran (Acros Organics) was distilled from Na and benzophenone. Anhydrous 2-propanol was purchased form Acros Organics. Thioredoxin reductase, EDTA, 5,5′-dithio-bis-(2-nitrobenzoic acid), bovine serum albumin, and NADPH were obtained from Sigma-Aldrich. Bio-Gel P2 resin and Bradford reagent dye were obtained from BioRad, Incorporated. Apoptosis Kit #2 was purchased from Invitrogen. Cell-titer blue reagent was purchased from Promega. All other commercial reagents, including 5-indoleboronic acid pinacol ester and 1-methylindole-5-boronic acid pinacol ester used for synthetic procedures were purchased from Sigma-Aldrich or Strem Chemicals and were used without further purification. All ^1H and ^{13}C NMR spectra were recorded on a Varian AS-600 spectrometer, at 400 and 150 MHz, respectively, using tetramethylsilane as the internal standard. Mass spectral analyses were performed using the Ohio State University Analytical Facility. ^{31}P NMR spectra were recorded on Varian AS-400 and -600 spectrometers. Purity of all biologically active compounds was >95% as judged by microcombustion analyses (C, H, N, P, and Au) performed by Robertson Microlit Laboratories (Ledgewood, NJ). In addition, purity was >95% as judged by high-performance liquid chromatography. Reverse phase-HPLC used a linear gradient of 25% acetonitrile in water to 100% acetonitrile over a 25 min with a flow rate of 1 mL/min monitored at 220 and 280 nm using a Vadac C18 column; 4.6 mm × 250 mm. RP-HPLC was performed using a JASCO analytical HPLC system.

*tert-Butyl 5-(4,4,5,5-Tetramethyl-1,3,2-dioxaborolan-2-yl)-1H-indole-1-carboxylate (**1**).* 5-Indoleboronic acid pinacol ester (1.5 g, 6.1 mmol) was treated with *tert*-butoxycarbonyl [$(Boc)_2O$](2.02 g, 9.3 mmol) in the presence of dimethylaminopyridine (148 mg, 1.2 mmol) in 20 mL of anhydrous CH_3CN. The reaction was stirred until completion, which was monitored by thin layer chromatography. After completion, the crude product **1** was concentrated in vacuo then purified through flash chromatography (silica gel, hexanes/EtOAc 9:1) to produce a white solid in 90% yield. ^1H NMR (400 MHz, $CDCl_3$) δ (ppm): 8.15–8.13 (m, 1H), 8.05 (m, 1H), 7.74–7.76 (m, 1H), 6.56–6.57 (d, J = 4.0 Hz, 1H), 1.67 (s, 9H), 1.37 (s, 12H). ^{13}C NMR (150 MHz, $CDCl_3$, ppm) δ: 149.91, 130.74, 130.36, 128.44, 126.09, 107.74, 83.95, 28.40, 25.12.

*(5-(4,4,5,5-Tetramethyl-1,3,2-dioxaborolan-2-yl)-1H-indol-1-yl)-methyl Pivalate (**2**).* To a solution of 5-indoleboronic acid pinacol ester (350 mg, 1.45 mmol) in 10 mL of anhydrous THF was added sodium hydride (63 mg, 2.17 mmol). After the solution was stirred for 30 min, the reaction was chilled to 0 °C, and then pivaloyloxymethyl chloride (433 mg, 2.17 mmol) was added dropwise. The reaction was stirred for 4 h. After completion, the reaction was quenched with ice–water and extracted with EtOAc, washed with brine, and dried over anhydrous magnesium sulfate. The solution was then gravity filtered and concentrated under reduced pressure. The residue was then purified by silica gel flash chromatography, eluting with hexanes/EtOAc (9:1) to yield a white solid at a 54% yield. ^1H NMR (400 MHz, $CDCl_3$) δ (ppm): 8.13 (m, 1H), 7.72–7.69 (m, 1H), 7.50–7.48 (m, 1H), 7.32–7.24 (m, 1H), 6.54–6.52 (m, 1H), 6.09 (s, 2H), 1.37 (s, 12H), 1.12 (s, 9H). ^{13}C NMR (150 MHz, $CDCl_3$) δ (ppm): 178.42, 138.41, 129.00, 128.79, 109.21, 104.18, 83.74, 68.82, 39.13, 29.93, 27.12, 25.11.

General Procedure for the Indole Gold(I)–Phosphine Ligand Scaffolds. To a round-bottom flask, compound **1** or **2** (350 mg, 1 equiv), cesium carbonate (653 mg, 2 equiv), and (phosphine)gold(I) complex ($BrAuPPh_3$) [320 mg, 0.5 equiv] were added, followed by 10 mL of anhydrous isopropyl alcohol. The reaction was heated at 40 °C for 16 h. After completion of the reaction, the mixture was concentrated in vacuo. To the crude solid was then added toluene, and the residue was filtered through Celite. The solution was concentrated under reduced pressure. The crude residue was precipitated from *n*-pentane.

*[5-{Triphenylphosphine–Gold(I)}–tert-Butyl 1H-indole-1-carboxylate] (**3**).* White solid, 51% yield. ^1H NMR (400 MHz, C_6D_6) δ (ppm): 8.37–8.35 (d, J = 5.2 Hz, 1H), 8.24–8.21 (dd, J = 5.2, 7.6 Hz, 1H), 7.46–7.42 (m, 6H), 6.98–6.97 (m, 1H), 6.96–6.90 (m, 9H), 6.52–6.51 (m, 1H), 1.35 (s, 9H), $^{31}P\{^1H\}$ NMR (243 MHz, C_6D_6) δ (ppm): 44.66. $^{13}C\{^1H\}$ NMR (158 MHz, $CDCl_3$) δ (ppm): 165.88–165.10, 135.61, 134.68–134.59, 131.58, 131.29, 129.26–129.19, 128.44, 125.51, 124.50, 114.31, 107.94, 28.49. (TOF MS-ES+): calculated m/z = 698.1499; found 698.1503 [M + Na]; m/z = $[Au(PPh_3)_2]$ = 721.1484.

*[5-{Tricyclohexylphosphine–Gold(I)}–tert-Butyl 1H-indole-1-carboxylate] (**4**).* White solid, 50% yield. ^1H NMR (400 MHz, $CDCl_3$) δ (ppm): 7.99 (m, 1H), 7.70–7.69 (m, 1H), 7.46 (m, 2H), 6.47–6.46 (m, 1H), 2.06–2.04 (m, 10H), 1.87–1.86 (m, 7H), 1.74–1.73 (m, 3H), 1.65 (s, 9H), 1.37–1.25 (m, 12H), 0.895–0.870 (m, 1H). $^{31}P\{^1H\}$ NMR (243 MHz, C_6D_6) δ (ppm): 58.09. $^{13}C\{^1H\}$ NMR (150 MHz, $CDCl_3$) δ (ppm): 170.23–169.50, 135.16, 131.16, 124.82, 114.23, 107.97, 33.55–33.39, 30.93, 28.48, 27.5–27.43, 26.30. (TOF MS-ES+): calculated m/z = 716.2908; found 716.2897 [M + Na].

*[5-{[1,1′-Biphenyl]-2-yldicyclohexylphosphine aurate(I)}–tert-Butyl H-indole-1-carboxylate] (**5**).* White solid, 52% yield. ^1H NMR (400 MHz, C_6D_6) δ (ppm): 8.12–8.10 (d, J = 8.0 Hz, 1H), 7.94–7.91

(dd, J = 4.8, 8.0 Hz, 1H), 7.61−7.57 (m, 1H), 7.28−7.27 (m, 5H), 7.21−7.19 (m, 1H), 7.10−7.08 (m, 4H), 6.57−6.56 (m, 1H), 1.99−1.94 (m, 4H), 1.70−1.60 (m, 3H), 1.51 (m, 4H), 1.46−1.43 (m,3H), 1.38 (s, 9H), 1.05−0.88 (m, 8H). $^{31}P\{^1H\}$ NMR (243 MHz, C_6D_6) δ (ppm): 52.31. $^{13}C\{^1H\}$ NMR (150 MHz, $CDCl_3$) δ (ppm): 167.51−166.76, 149.36−149.29, 142.18, 135.56, 135.35−135.30, 132.37−132.33, 131.19, 130.23, 129.73, 128.50, 128.30, 128.02, 127.39, 124.14, 113.80, 107.97, 36.82−36.65, 31.14−31.10, 29.77, 28.51, 27.03−26.95, 26.08. (TOF MS-ES+): calculated m/z = 786.2751; found 786.2722 [M + Na].

*[5-{[1,1′-Biphenyl]-2-yldicyclohexylphosphine aurate(I)}−(1H-Indol-1-yl)methyl pivalate] (**6**).* White solid, 50% yield. ^1H NMR (400 MHz, $CDCl_3$) δ (ppm): 8.21−7.86 (m, 1H), 7.58−7.57 (m, 1H), 7.44−7.42 (m, 5H), 7.48−7.32 (m, 1H), 7.29−7.26 (m, 4H), 7.08−7.07 (m, 1H), 6.40−6.39 (m, 1H), 6.03 (s, 2H), 2.35−2.16 (m, 2H), 2.11−1.95 (m, 2H), 1.64−1.54 (m, 5H), 1.52−1.51 (m, 6H), 1.31−1.41 (m,7H), 1.10 (s, 9H). $^{31}P\{^1H\}$ NMR (243 MHz, $CDCl_3$) δ (ppm): 53.80. $^{13}C\{^1H\}$ NMR (150 MHz, $CDCl_3$) δ (ppm): 178.62, 164.69−163.99, 149.19−149.12, 142.17, 135.76−135.69, 135.34, 133.67, 132.34−132.29, 131.13, 130.21, 129.73, 129.52−129.33, 128.61−128.41, 128.47,128.17, 128.01, 127.36, 126.83, 108.37, 103.46, 69.21, 39.14, 36.84, 31.15, 29.90−29.81, 27.18−26.82, 26.06, 25.99−25.07. (TOF MS-ES+): calculated m/z = 800.2908; found 800.2902 [M + Na].

*[5-{[1,1′-Biphenyl]-2-yldicyclohexylphosphine aurate(I)}−1-Methyl-1H-indole] (**7**).* White solid, 62% yield. ^1H NMR (400 MHz, C_6D_6) δ (ppm): 8.27−8.26 (d, J = 8 Hz, 1H), 7.90−7.87 (dd, J = 4.4, 7.6 Hz, 1H), 7.74−7.69 (m, 1H), 7.30−7.27 (m, 5H), 7.10−7.05 (m, 4H), 6.68−6.69 (m, 1H), 6.64-.6.63 (m, 1H), 3.06 (s,3H) 1.98−1.92 (m, 4H), 1.72−1.70 (m, 2H), 1.57−1.43 (m,10H), 0.97 (m,6H). $^{31}P\{^1H\}$ NMR (243 MHz, C_6D_6) δ (ppm): 53.45. $^{13}C\{^1H\}$ NMR (150 MHz, $CDCl_3$) δ (ppm): 163.19−162.43, 149.17−147.10, 142.17, 135.96−135.84, 132.82, 132.32−132.27, 131.00, 129.73, 128.93−128.89, 128.56−128.33, 128.48, 128.02, 127.34−127.28, 127.01, 108.00, 100.49, 36.85−36.68, 32.77, 31.20−31.16, 29.83, 27.05−26.96, 26.08. (TOF MS-ES+): calculated m/z = 700.2383; found 700.2382 [M + Na].

General Cell Culture Procedures. HeLa, MCF-7, HCT-116, and CEM-C7 were obtained from the American Type Culture Collection (Manassas, VA). All adherent cell lines were maintained in Dulbecco's modified Eagle's medium (Mediatech) with 100 U/mL penicillin (Invitrogen), 100 μg/mL streptomycin (Invitrogen), 0.25 μg/mL amphotericin B (Invitrogen), and 10% fetal bovine serum (USA Scientific) and incubated at 37 °C with 5% CO_2. CEM cells were maintained in RPMI-1640 media supplemented with 100 U/mL penicillin, 100 μg/mL streptomycin, 0.25 μg/mL amphotericin B, and 10% fetal bovine serum and incubated at 37 °C with 5% CO_2.

Cell Proliferation Assays. Cells were plated at a density of 7000−13 000/well in 200 μL of media overnight in a 96-well plate. Each (phosphine)gold(I)−indole was added to wells in a dose-dependent manner (0.01−100 μM). Cells were treated with compounds for variable time periods (8−48 h). With adherent cell lines, medium was removed from the wells and then 100 μL of fresh medium was added into each well followed by the addition of 20 μL of cell titer-blue reagent (Promega). Cells were incubated with reagent for 1−4 h, and the optical density of samples was read at 560 nm using a microplate reader. The background absorbance of dye with media was subtracted from each sample. Cell viability was then normalized against cells treated with DMSO. IC_{50} values were obtained using a fit of the data to eq 1

$$y = 100\%/[1 + (IC_{50}/\text{inhibitor})] \quad (1)$$

where y is the fraction of viable cells, IC_{50} is the concentration of inhibitor that inhibits 50% cell growth, and inhibitor is the concentration of compound tested. Each experiment represents an average of at least three independent determinations performed on different days.

Measurements of Apoptosis. Cells were plated at 200 000/mL, and Au(I)−indole analogues were added in a dose-dependent fashion for 12−24 h. Cells were trypsinized and then washed with cold PBS. After the supernatant was discarded, a 100 μL solution containing 1X annexin-binding buffer, 5 μL of Alexa Fluor 488 annexin V, and 1 μg/mL PI solution was added to each sample. The cells were incubated at room temperature for 15 min. After this incubation period, an additional 400 μL of 1X annexin-binding buffer was added. Cells were analyzed using band-pass filters with wavelengths of 525/40 nm and 620/30 nm with a Beckman Coulter XL flow cytometer.

Cell Cycle Analyses. Cells were plated at a density of 200 000/mL. Au(I)−indole analogues were then added in a dose-dependent manner for time periods varying from 1 to 3 days. Cells were treated with 0.25% trypsin and harvested by centrifugation. The supernatant was removed and then washed with PBS. After aspiration of PBS, 500 μL of 70% ethanol was added and cells were incubated on ice for 15 min followed by centrifugation and the removal of ethanol. One milliliter of PI staining solution [(10 mL of 0.1 Triton X-100/PBS, 0.4 mL of 500 μg/mL of PI, and 2 mg/mL of DNase-free RNase)] was added to the cell suspension, placed on ice for 30 min, and then analyzed using a Beckman Coulter XL flow cytometer with a red filter. Each experiment represents an average of three independent determinations performed on different days.

Microscopy. Cells were plated at 75 000−125 000/mL for 24 h. (Phosphine)gold(I)−indoles then were added at concentrations equal to their LD_{50} values for 12 and 24 h. Alexa Fluor 488 annexin V and propidium iodide were added to each well, and images were taken on Leica CTR 6500 microscope using green (480/40 nm) and red (560/40 nm) excitation band-pass filters.

Clonogenic Survival Assay. HeLa cells were plated at a density of 250 000−300 000 cells/mL. After 24 h cells, the cells were irradiated in a dose-dependent manner (0−4 Gy) using a ^{137}Cs gamma source. After treatment, the cells were trypsinized and plated at a density between 300 and 4000 cells in 60 mm dishes. Cells were allowed to grow colonies (1 colony ≥ 50 cells) for 10−14 days, stained with 0.25% crystal violet, and manually counted to measure the number of colonies. Survival fractions were normalized against positive controls (colony formation with no radiation) and plotted as the log percent survival versus dose of radiation. Each experiment was performed an average of four times with cells propagated on several different days.

Detection of γH2AX Formation. HeLa cells were plated at a density of 40 000 cells/mL in 24-well glass bottom plate for 24 h. After this time, cells were treated with Au(I)−indole compounds at the desired concentration for an additional 24 h. The cells were irradiated at 2 Gys. Cells were fixed with 4% paraformaldehyde for 15 min at 37 °C at time points corresponding to 0.5, 1, 2, and 4 h. Cells were washed with 1X PBS and permeabilized in 0.2% Triton X-100 for 15 min at 37 °C. Cells were washed with 1X PBS and subsequently blocked with 1% BSA, 0.1% Tween in 1X PBS for 1 h at room temperature. Mouse monoclonal antiphospho-histone H2AX antibody (Millipore) was applied (1:500 dilution) to each well for 1 h. After washing several times with blocking buffer, a 1:500 dilution of goat antimouse secondary antibody conjugated with Alexa 647 (Invitrogen) was added for 1 h. The wells were then washed several times, and the number of γH2AX foci per nuclei was measured using an iCyte laser scanning cytometer with a red long pass filter (650 nm). To collect accurate data, a threshold was set to minimize noise produced by unrelated events using iNovator software (version 3.4.2.52). Each well was scanned using a 40× magnification with 0.25 μm × step and a field size of 250 × 186 μm (1000 × 768 pixels). Data were plotted as the percentage of cells as a function of foci number. The resulting histogram was fit to the equation for a Gaussian distribution (eq 2).

$$y = 1/(2\pi\sigma^2)^{1/2}{}_e{}^{-[(\chi-m)2/2\sigma2]} \quad (2)$$

where y is the percentage of cells, μ is the mean, and σ is the variance used to define the width of the mean.

Reactivity of Au(I) Compounds with Biological Thiols. BSA concentrations were determined measuring A_{280} (ε =36 600 M^{-1} cm^{-1}) or using the Bradford assay measuring samples at A_{595} as described.[73] The SH titer of BSA was determined using DTNB (ε_{414} = 13 600 M^{-1} cm^{-1}) as previously described.[74] BSA (0−120 μM) was treated with variable concentrations of compound **3** (120 μM) and

compound **4** (120 μM), yielding Au(I)/BSA ratios of 4:1, 2:1, 1:1, and 0:1. Phosphate-buffered saline (PBS) was used as the buffer in these experiments. After incubation for 1 h at 37 °C, the reaction mixtures were applied to Penefsky spun columns using Bio-Gel P2 gel filtration resin and centrifugal force to rapidly and efficiently separate unreacted Au(I)-containing complexes from BSA. Penefsky spun columns were prepared using the following procedure: P2 resin was preswelled in 10 mM Tris, pH 7.5, and 1 mM EDTA. The resin was then loaded into 1 mL tuberculin syringes (Becton-Dickinson) and spun in a fixed-angle rotor at 2000 rpm for 2 min. Reaction mixtures described above were then loaded into the column and spun at 2000 rpm for 2 min. The eluants were removed and analyzed for Au(I)-containing compounds and BSA. Compound **3** and compound **4** were analyzed measuring absorbances at 212 and 280 nm before and after spinning through the Penefsky column. Note that these experiments were performed in the absence of BSA; thus, there is no spectral overlap between the Au(I) complexes and protein. In all cases, free Au(I)-containing complexes were retained in the P2 resin, as their presence was not detected in the eluant. The concentration of BSA was quantified before and after spinning through the Penefsky column using Bradford assay dye. In these cases, the concentration of BSA was reduced less than 5% after elution through the Penefsky column. This result indicates that BSA was not retained in the P2 resin under these conditions. In some experiments, a wavelength of 319 nm was used to quantify the presence of Au(I)−indole compounds when the Au(I)−indole (compound **3**) was incubated with BSA. This higher wavelength avoids spectral overlap with protein. Finally, the SH titer of BSA before and after elution through the Penefsky column was determined using DTNB (ε_{414} = 13 600 M^{-1} cm^{-1}) as described.[74]

Interactions of compound **3** with cysteine were measured via the quantitation of reactive sulfhydryls using DTNB (ε_{414} = 13 600 M^{-1} cm^{-1}) as previously described.[74] A linear standard curve for L-cysteine was measured by reacting variable concentrations of L-cysteine (0−800 μM) with 2 mM DTNB at 37 °C for 60 min. PBS was used as the reaction buffer. The reactivity of DTNB was measured using an absorbance of 412 nm (ε_{414} = 13 600 M^{-1} cm^{-1}). Incubation of 400 μM L-cysteine with an equivalent concentration of compound **3** does not change the titer of free SH present on L-cysteine.

Inhibitory Effects of Au(I) Compounds against Thioredoxin Reductase. The inhibitory effects of compound **3**, compound **4**, and the unprotected Au(I)−phosphine ligands ($BrAuPPh_3$ and BrAuPCy3) were measured against rat liver TrxR. All assays were performed at 25 °C. Experiments were performed, adding 600 nM TrxR to a preincubated solution containing 100 mM potassium phosphate, pH 7.0, 10 mM EDTA, 5 mM 5,5′dithiobis(2-nitrobenzoic acid) (DTNB), 0.2 mg/mL BSA, and 240 μM NADPH in the absence and presence of Au(I)-containing compounds. The amount of TNB formed as a function of time was measured by examining changes in absorbance at 412 nm. Under all conditions tested, the change in absorbance was linear under the time frame tested (5 min). Time courses in product formation were fit using eq 3

$$y = mt \tag{3}$$

where y is the change in absorbance at 412 nm, m is the rate of the reaction, and t is time.

Computations. Spin-unrestricted density-functional theory computations were performed within the Gaussian 03 program suite.[75] Calculations employed the exchange functional of Becke[76] and the correlation functional of Lee, Yang, and Parr.[77] Nonmetal atoms were described with the TZVP basis set of Godbelt, Andzelm, and coworkers.[78] Gold orbitals were described with the Stuttgart effective core potential and the associated basis set.[79] Gas-phase equilibrium geometries were optimized in redundant internal coordinates without imposed symmetry. Harmonic frequency calculations confirm the structures so generated to be energy minima. All other calculated properties reported here include implicit water solvation, which was incorporated in single-point calculations of the gas-phase geometries with Tomasi's polarizable continuum model.[80]

■ ASSOCIATED CONTENT

Ⓢ Supporting Information

Details regarding the characterization of each compound using ^{1}H NMR, ^{13}C NMR, ^{31}P NMR, and mass spectroscopy. The crystal structure of compound **3**. Data for the reactivity of compound **3** with BSA or cysteine. This material is available free of charge via the Internet at http://pubs.acs.org.

■ AUTHOR INFORMATION

Corresponding Author

*Tel: (216)-368-4723, fax: (216) 368-3395, e-mail: ajb15@cwru.edu (A.J.B.); tel: (216) 368-0991, fax: (216) 368-3006, e-mail: tgray@case.edu (T.G.).

■ ACKNOWLEDGMENTS

T.G.G. thanks the National Science Foundation (grant CHE-1057659) and the Alfred P. Sloan Foundation for support. A.J.B. is supported by funding from the National Institutes of Health (CA118408) and the Department of Defense, US Army Medical Research (CA091380). We thank Nihal Deligonul for assistance with the X-ray diffraction crystallography.

■ ABBREVIATIONS USED

TrxR, thioredoxin reductase; DSBs, double-strand DNA breaks; IC_{50}, concentration of a compound that inhibits 50% cell growth; LD_{50}, concentration of compound required to kill 50% of members of a tested population after a specified time period; FACS, fluorescence-activated cell sorting; PI, propidium iodide; G1, period in the cell cycle during interphase; G2, phase of the cell cycle following the successful completion of S-phase and that precedes mitosis; M, phase of the cell cycle where mitosis occurs; S-phase, phase of the cell cycle in which genomic DNA is replicated; sub-G1, discontinuous fragmentation of nuclear DNA during apoptosis; BSA, bovine serum albumin; DTNB, 5,5′-dithiobis(dinitrobenzoic acid); EDTA, ethylenediaminetetraacetate sodium salt; Gy, SI unit of absorbed radiation; ATM, Ataxia telangiectasia mutated; ATR, Ataxia telangiectasia and Rad3 related; DNA-PK, DNA-dependent protein kinase; cdk, cyclin-dependent kinase; γ-H2AX, a phosphorylated form of histone H2A; PBS, phosphate-buffered saline

■ REFERENCES

(1) Cowan, J. A. Structural and catalytic chemistry of magnesium-dependent enzymes. *Biometals* **2002**, *15*, 225−235.
(2) Qi, W.; Cowan, J. A. Structural, Mechanistic and Coordination Chemistry of Relevance to the Biosynthesis of Iron-Sulfur and Related Iron Cofactors. *Coord. Chem. Rev.* **2011**, *255*, 688−699.
(3) Brown, K. L. The enzymatic activation of coenzyme B12. *Dalton Trans.* **2006**, 1123−1133.
(4) Brewer, G. J. Risks of copper and iron toxicity during aging in humans. *Chem. Res. Toxicol.* **2010**, *23*, 319−326.
(5) Moulis, J. M. Cellular mechanisms of cadmium toxicity related to the homeostasis of essential metals. *Biometals* **2010**, *23*, 877−896.
(6) Butterworth, R. F. Metal toxicity, liver disease and neurodegeneration. *Neurotox. Res.* **2010**, *18*, 100−105.
(7) Brabec, V.; Kasparkova, J. Modifications of DNA by platinum complexes. Relation to resistance of tumors to platinum antitumor drugs. *Drug Resist. Update* **2005**, *8*, 131−146.
(8) Wang, X. Fresh platinum complexes with promising antitumor activity. *Anticancer Agents Med. Chem.* **2010**, *10*, 396−411.
(9) Fléchon, A.; Rivoire, M.; Droz, J. P. Management of advanced germ-cell tumors of the testis. *Nat. Clin. Pract. Urol.* **2008**, *5*, 262−276.
(10) Adams, G.; Zekri, J.; Wong, H.; Walking, J.; Green, J. A. Platinum-based adjuvant chemotherapy for early-stage epithelial

ovarian cancer: single or combination chemotherapy? *BJOG* **2010**, *117*, 1459−1467.
(11) Rubbiani, R.; Kitanovic, I.; Alborzinia, H.; Can, S.; Kitanovic, A.; Onambele, L. A.; Stefanopoulou, M.; Geldmacher, Y.; Sheldrick, W. S.; Wolber, G.; Prokop, A.; Wölfl, S.; Ott, I. Benzimidazol-2-ylidene gold(I) complexes are thioredoxin reductase inhibitors with multiple antitumor properties. *J. Med. Chem.* **2010**, *53*, 8608−8618.
(12) Yan, K.; Lok, C. N.; Bierla, K.; Che, C. M. Gold(I) complex of N,N′-disubstituted cyclic thiourea with in vitro and in vivo anticancer properties-potent tight-binding inhibition of thioredoxin reductase. *Chem. Commun. (Cambridge, U. K.).* **2010**, *46*, 7691−7693.
(13) Vergara, E.; Casini, A.; Sorrentino, F.; Zava, O.; Cerrada, E.; Rigobello, M. P.; Bindoli, A.; Laguna, M.; Dyson, P. J. Anticancer therapeutics that target selenoenzymes: synthesis, characterization, in vitro cytotoxicity, and thioredoxin reductase inhibition of a series of gold(I) complexes containing hydrophilic phosphine ligands. *ChemMedChem* **2010**, *5*, 96−102.
(14) Maiore, L.; Cinellu, M. A.; Michelucci, E.; Moneti, G.; Nobili, S.; Landini, I.; Mini, E.; Guerri, A.; Gabbiani, C.; Messori, L. Structural and solution chemistry, protein binding and antiproliferative profiles of gold(I)/(III) complexes bearing the saccharinato ligand. *J. Inorg. Biochem.* **2011**, *105*, 348−355.
(15) Zhang, X.; Frezza, M.; Milacic, V.; Ronconi, L.; Fan, Y.; Bi, C.; Fregona, D.; Dou, Q. P. Inhibition of tumor proteasome activity by gold-dithiocarbamato complexes via redox-dependent *and* -independent processes. *J. Cell Biochem.* **2010**, *109*, 162−172.
(16) Trani, M.; Sorrentino, A.; Busch, C.; Landström, M. Pro-apoptotic effect of aurothiomalate in prostate cancer cells. *Cell Cycle* **2009**, *8*, 306−313.
(17) Shaw, C. F. III. Gold-based therapeutic agents. *Chem. Rev.* **1999**, *99*, 2589−2600.
(18) Ho, S. Y. Tiekink, E. R. T. ^{79}Au Gold-Based Metallotherapeutics: Use and Potential. In *Metallotherapeutic Drugs & Metal-based Diagnostic Agents: The Use of Metals in Medicine*; Gielen, M.; Tiekink, E. R. T., Eds.; Wiley: New York, 2005; pp 507−528.
(19) Crooke, S. T.; Mirabelli, C. K. Molecular mechanisms of action of auranofin and other gold complexes as related to their biologic activities. *Am. J. Med.* **1983**, *75*, 109−113.
(20) Mirabelli, C. K.; Johnson, R. K.; Hill, D. T.; Faucette, L. F.; Girard, G. R.; Kuo, G. Y.; Sung, C. M.; Crooke, S. T. Correlation of the in vitro cytotoxic and in vivo antitumor activities of gold(I) coordination complexes. *J. Med. Chem.* **1986**, *29*, 218−223.
(21) Messori, L.; Marcon, G. Gold complexes in the treatment of rheumatoid arthritis. *Met. Ions Biol. Syst.* **2004**, *249*, 279−304.
(22) Ward, J. R. Role of disease-modifying antirheumatic drugs versus cytotoxic agents in the therapy of rheumatoid arthritis. *Am. J. Med.* **1988**, *85*, 39−44.
(23) Simon, T. M.; Kunishima, D. H.; Vibert, G. J.; Lorber, A. Cellular antiproliferative action exerted by auranofin. *J. Rheumatol. Suppl.* **1979**, *5*, 91−97.
(24) Bhabak, K. P.; Bhuyan, B. J.; Mugesh, G. Bioinorganic and medicinal chemistry: aspects of gold(I)-protein complexes. *Dalton Trans.* **2011**, *40*, 2099−2111.
(25) Rigobello, M. P.; Scutari, G.; Folda, A.; Bindoli, A. Mitochondrial thioredoxin reductase inhibition by gold(I) compounds and concurrent stimulation of permeability transition and release of cytochrome c. *Biochem. Pharmacol.* **2004**, *67*, 689−696.
(26) de Sa Alves, F. R.; Barreiro, E. J.; Fraga, C. A. M. From nature to drug discovery: The indole scaffold as a 'privleged structure'. *Mini Rev. Med. Chem.* **2009**, *9*, 782−793.
(27) Fuse, E.; Kuwabara, T.; Sparreboom, A.; Sausville, E. A.; Figg, W. D. Review of UCN-01 development: a lesson in the importance of clinical pharmacology. *J. Clin. Pharmacol.* **2005**, *45*, 394−403.
(28) Weng, J. R.; Omar, H. A.; Kulp, S. K.; Chen, C. S. Pharmacological exploitation of indole-3-carbinol to develop potent antitumor agents. *Mini Rev. Med. Chem.* **2010**, *10*, 398−404.
(29) Giroux, V.; Dagorn, J. C.; Iovanna, J. L. A review of kinases implicated in pancreatic cancer. *Pancreatology* **2009**, *9*, 738−754.
(30) Shaw, C.F. III. The protein chemistry of antiarthritic gold(I) thiolates and related complexes. *Comments Inorg. Chem.* **1989**, *8*, 233−267.
(31) Partyka, D. V.; Zeller, M.; Hunter, A. D.; Gray, T. G. Relativistic functional groups: aryl carbon-gold bond formation by selective transmetalation of boronic acids. *Angew. Chem., Int. Ed.* **2006**, *45*, 8188−8191.
(32) Gao, L.; Peay, M. A.; Partyka, D. V.; Updegraff, J. B. III; Teets, T. S.; Esswein, A. J.; Zeller, M.; Hunter, A. D.; Gray, T. G. Mono- and di-gold(I) naphthalenes and pyrenes: synthesis, crystal structures, and photophysics. *Organometallics* **2009**, *28*, 5669−5681.
(33) Partyka, D. V.; Updegraff, J. B. III; Zeller, M.; Hunter, A. D.; Gray, T. G. Probing the steric limits of carbon-gold bond formation: (Dialkylbiarylphosphine)gold(I) aryls. *Organometallics* **2009**, *28*, 1666−1674.
(34) Harvey, A. L.; Cree, I. A. High-throughput screening of natural products for cancer therapy. *Planta Med.* **2010**, *76*, 1080−1086.
(35) Willingham, M. C. Cytochemical methods for the detection of apoptosis. *J. Histochem. Cytochem.* **1999**, *47*, 1101−1109.
(36) Shaw, C. F. III; Isab, A. A.; Coffer, M. T.; Mirabelli, C. K. Gold(I) efflux from auranofin-treated red blood cells. Evidence for a glutathione-gold-albumin metabolite. *Biochem. Pharmacol.* **1990**, *40*, 1227−1234.
(37) Shaw, C. F. III; Isab, A. A.; Hoeschele, J. D.; Starich, M.; Locke, J.; Schulteis, P.; Xiao, J. Oxidation of the phosphine from the auranofin analogue, triisopropylphosphine(2,3,4,6-tetra-*O*-acetyl-1-thio-*β*-D-glucopyranosato-S)gold(I), via a protein-bound phosphonium intermediate. *J. Am. Chem. Soc.* **1994**, *116*, 2254−2260.
(38) Roberts, J. R.; Xiao, J.; Schliesman, B.; Parsons, D. J.; Shaw, C. F. III. Kinetics and mechanism of the reaction between serum albumin and auranofin (and its isopropyl analogue) in vitro. *Inorg. Chem.* **1996**, *35*, 424−433.
(39) Holmgren, A. Thioredoxin structure and mechanism: conformational changes on oxidation of the active-site sulfhydryls to a disulfide. *Structure* **1995**, *3*, 239−243.
(40) Jester, B. W.; Cox, K. J.; Gaj, A.; Shomin, C. D.; Porter, J. R.; Ghosh, I. A coiled-coil enabled split-luciferase three-hybrid system: applied toward profiling inhibitors of protein kinases. *J. Am. Chem. Soc.* **2010**, *132*, 11727−11735.
(41) Carpinelli, P.; Moll, J. Aurora kinases and their inhibitors: more than one target and one drug. *Adv. Exp. Med. Biol.* **2008**, *610*, 54−73.
(42) Miglarese, M. R.; Carlson, R. O. Development of new cancer therapeutic agents targeting mitosis. *Expert Opin. Investig. Drugs* **2006**, *15*, 1411−1425.
(43) Katayama, H.; Sen, S. Aurora kinase inhibitors as anticancer molecules. *Biochim. Biophys. Acta* **2010**, *1799*, 829−839.
(44) Carrière, A.; Cargnello, M.; Julien, L. A.; Gao, H.; Bonneil, E.; Thibault, P.; Roux, P. P. Oncogenic MAPK signaling stimulates mTORC1 activity by promoting RSK-mediated raptor phosphorylation. *Curr. Biol.* **2008**, *18*, 1269−1277.
(45) Kang, S.; Elf, S.; Lythgoe, K.; Hitosugi, T.; Taunton, J.; Zhou, W.; Xiong, L.; Wang, D.; Muller, S.; Fan, S.; Sun, S. Y.; Marcus, A. I.; Gu, T. L.; Polakiewicz, R. D.; Chen, Z. G.; Khuri, F. R.; Shin, D. M.; Chen, J. p90 ribosomal S6 kinase 2 promotes invasion and metastasis of human head and neck squamous cell carcinoma cells. *J. Clin. Invest.* **2010**, *120*, 1165−1177.
(46) Tibbles, L. A.; Ing, Y. L.; Kiefer, F.; Chan, J.; Iscove, N.; Woodgett, J. R.; Lassam, N. J. MLK-3 activates the SAPK/JNK and p38/RK pathways via SEK1 and MKK3/6. *EMBO J.* **1996**, *15*, 7026−7035.
(47) Patyna, S.; Laird, A. D.; Mendel, D. B.; O'Farrell, A. M.; Liang, C.; Guan, H.; Vojkovsky, T.; Vasile, S.; Wang, X.; Chen, J.; Grazzini, M.; Yang, C. Y.; Haznedar, J. O.; Sukbuntherng, J.; Zhong, W. Z.; Cherrington, J. M.; Hu-Lowe, D. SU14813: a novel multiple receptor tyrosine kinase inhibitor with potent antiangiogenic and antitumor activity. *Mol. Cancer Ther.* **2006**, *5*, 1774−1782.
(48) Omuro, A. M. Exploring multi-targeting strategies for the treatment of gliomas. *Curr. Opin. Investig. Drugs* **2008**, *9*, 1287−1295.

(49) Rodon, J.; Perez, J.; Kurzrock, R. Combining targeted therapies: practical issues to consider at the bench and bedside. *Oncologist* **2010**, *15*, 37−50.
(50) Lee, J. H.; Pyon, J. K.; Kim, D. W.; Lee, S. H.; Nam, H. S.; Kim, C. H.; Kang, S. G.; Lee, Y. J.; Park, M. Y.; Jeong, D. J.; Cho, M. K. Elevated c-Src and c-Yes expression in malignant skin cancers. *J. Exp. Clin. Cancer Res.* **2010**, *29*, 116.
(51) Koh, H. J.; Toyoda, T.; Fujii, N.; Jung, M. M.; Rathod, A.; Middelbeek, R. J.; Lessard, S. J.; Treebak, J. T.; Tsuchihara, K.; Esumi, H.; Richter, E. A.; Wojtaszewski, J. F.; Hirshman, M. F.; Goodyear, L. J. Sucrose nonfermenting AMPK-related kinase (SNARK) mediates contraction-stimulated glucose transport in mouse skeletal muscle. *Proc. Natl. Acad. Sci. U.S.A.* **2010**, *107*, 15541−15546.
(52) Zips, D.; Thames, H. D.; Baumann, M. New anticancer agents: *in vitro* and *in vivo* evaluation. *In Vivo* **2005**, *19*, 1−7.
(53) Derheimer, F. A.; Kastan, M. B. Multiple roles of ATM in monitoring and maintaining DNA integrity. *FEBS Lett.* **2010**, *584*, 3675−3681.
(54) Smith, J.; Tho, L. M.; Xu, N.; Gillespie, D. A. The ATM-Chk2 and ATR-Chk1 pathways in DNA damage signaling and cancer. *Adv. Cancer Res.* **2010**, *108*, 73−112.
(55) Rogakou, E. P.; Boon, C.; Redon, C.; Bonner, W. M. Megabase chromatin domains involved in DNA double-strand breaks *in vivo*. *J. Cell. Biol.* **1999**, *146*, 905−915.
(56) Stiff, T.; Walker, S. A.; Cerosaletti, K.; Goodarzi, A. A.; Petermann, E.; Concannon, P.; O'Driscoll, M.; Jeggo, P. A. ATR-dependent phosphorylation and activation of ATM in response to UV treatment or replication fork stalling. *EMBO J.* **2006**, *25*, 5775−82.
(57) Stiff, T.; O'Driscoll, M.; Rief, N.; Iwabuchi, K.; Löbrich, M.; Jeggo, P. A. ATM and DNA-PK function redundantly to phosphorylate H2AX after exposure to ionizing radiation. *Cancer Res.* **2004**, *64*, 2390−2396.
(58) Lillig, C. H.; Holmgren, A. Thioredoxin and related molecules--from biology to health and disease. *Antioxid. Redox. Signal.* **2007**, *9*, 25−47.
(59) Bagowski, C. P.; You, Y.; Scheffler, H.; Vlecken, D. H.; Schmitz, D. J.; Ott, I. Naphthalimide gold(I) phosphine complexes as anticancer metallodrugs. *Dalton Trans.* **2009**, *48*, 10799−10805.
(60) Suryadinata, R.; Sadowski, M.; Sarcevic, B. Control of cell cycle progression by phosphorylation of cyclin-dependent kinase (CDK) substrates. *Biosci. Rep.* **2010**, *30*, 243−255.
(61) Finch, S. C. Radiation-induced leukemia: lessons from history. *Best Pract. Res. Clin. Haematol.* **2007**, *20*, 109−118.
(62) Chandana, S. R.; Movva, S.; Arora, M.; Singh, T. Primary brain tumors in adults. *Am. Fam. Physician* **2008**, *77*, 1423−1430.
(63) Hricak, H. Cancer of the uterus: the value of MRI pre- and post-irradiation. *Int. J. Radiat. Oncol. Biol. Phys.* **1991**, *21*, 1089−1094.
(64) MacMahon, B. Epidemiology and the causes of breast cancer. *Int. J. Cancer* **2006**, *118*, 2373−2378.
(65) Ward, J. F. The yield of DNA double-strand breaks produced intracellularly by ionizing radiation: a review. *Int. J. Radiat. Biol.* **1990**, *57*, 1141−1150.
(66) Harrison, L.; Blackwell, K. Hypoxia and anemia: factors in decreased sensitivity to radiation therapy and chemotherapy? *Oncologist* **2004**, *9*, 31−40.
(67) Vaupel, P.; Kelleher, D. K.; Höckel, M. Oxygen status of malignant tumors: pathogenesis of hypoxia and significance for tumor therapy. *Semin. Oncol.* **2001**, *28*, 29−35.
(68) Berry, S. E.; Kinsella, T. J. Targeting DNA mismatch repair for radiosensitization. *Semin. Radiat. Oncol.* **2001**, *11*, 300−315.
(69) Grem, J. L. 5-Fluorouracil: forty-plus and still ticking. A review of its preclinical and clinical development. *Invest. New Drugs* **2000**, *18*, 299−313.
(70) Lawrence, T. S. Radiation sensitizers and targeted therapies. *Oncology (Williston Park, N. Y.)* **2003**, *17*, 23−28.
(71) Lyman, G. H. Impact of chemotherapy dose intensity on cancer patient outcomes. *J. Natl. Compr. Cancer Network* **2009**, *7*, 99−108.
(72) Blanksby, S. J.; Ellison, G. B. Bond dissociation energies of organic molecules. *Acc. Chem. Res.* **2003**, *36*, 255−263.
(73) Sapan, C. V.; Lundblad, R. L.; Price, N. C. Colorimetric protein assay techniques. *Biotechnol. Appl. Biochem.* **1999**, *29*, 99−108.
(74) Ellman, G. L. A colorimetric method for determining low concentrations of mercaptans. *Arch. Biochem. Biophys.* **1958**, *74*, 443−450.
(75) Frisch, M. J.; Trucks, G. W.; Schlegel, H. B.; Scuseria, G. E.; Robb, M. A.; Cheeseman, J. R.; Montgomery, J. A., Jr.; Vreven, T.; Kudin, K. N.; Burant, J. C.; Millam, J. M.; Iyengar, S. S.; Tomasi, J.; Barone, V.; Mennucci, B.; Cossi, M.; Scalmani, G.; Rega, N.; Petersson, G. A.; Nakatsuji, H.; Hada, M.; Ehara, M.; Toyota, K.; Fukuda, R.; Hasegawa, J.; Ishida, M.; Nakajima, T.; Honda, Y.; Kitao, O.; Nakai, H.; Klene, M.; Li, X.; Knox, J. E.; Hratchian, H. P.; Cross, J. B.; Bakken, V.; Adamo, C.; Jaramillo, J.; Gomperts, R.; Stratmann, R. E.; Yazyev, O.; Austin, A. J.; Cammi, R.; Pomelli, C.; Ochterski, J. W.; Ayala, P. Y.; Morokuma, K.; Voth, G. A.; Salvador, P.; Dannenberg, J. J.; Zakrzewski, V. G.; Dapprich, S.; Daniels, A. D.; Strain, M. C.; Farkas, O.; Malick, D. K.; Rabuck, A. D.; Raghavachari, K.; Foresman, J. B.; Ortiz, J. V.; Cui, Q.; Baboul, A. G.; Clifford, S.; Cioslowski, J.; Stefanov, B. B.; Liu, G.; Liashenko, A.; Piskorz, P.; Komaromi, I.; Martin, R. L.; Fox, D. J.; Keith, T.; Al-Laham, M. A.; Peng, C. Y.; Nanayakkara, A.; Challacombe, M.; Gill, P. M. W.; Johnson, B.; Chen, W.; Wong, M. W.; Gonzalez, C.; and Pople, J. A. *Gaussian 03, Revision D.01*, Gaussian, Inc., Wallingford, CT, 2004.
(76) Becke, A. D. Density-functional exchange-energy approximation with correct asymptotic behavior. *Phys. Rev. A* **1988**, *38*, 3098−3100.
(77) Lee, C.; Yang, W.; Parr, R. Development of the Colle-Salvetti correlation-energy formula into a functional of the electron density. *Phys. Rev. B* **1988**, *37*, 785−789.
(78) Godbout, N.; Salahub, D. R.; Andzelm, J.; Wimmer, E. Optimization of gaussian-type basis sets for local spin density functional calculations. Part I. Boron through neon, optimization technique and validation. *Can. J. Chem.* **1992**, *70*, 560−571.
(79) Dolg, M.; Wedig, U.; Stoll, H.; Preuss, H. Energy-adjusted ab initio pseudopotentials for the first row transition elements. *J. Chem. Phys.* **1987**, *86*, 866−872.
(80) Miertus, S.; Scrocco, E.; Tomasi, J. Electrostatic interaction of a solute with a continuum. A direct utilization of ab initio molecular potentials for the prevision of solvent effects. *Chem. Phys.* **1981**, *55*, 117−129.